with combined heterozygous mutations in Pdx-1, Hnf-1α, and Hnf-3β. Proc Natl Acad Sci U S A 99:3818–3823
31. Nishikawa T, Sasahara T, Kiritoshi S et al (2003) Evaluation of urinary 8-hydroxydeoxy-guanosine as a novel biomarker of macrovascular complications in type 2 diabetes. Diabetes Care 26:1507–1512
32. Kaneto H, Kajimoto Y, Miyagawa J et al (1999) Beneficial effects of antioxidants in diabetes. Possible protection of pancreatic beta cells against glucose toxicity. Diabetes 48:2398–2406
33. Eiki J, Nagata Y, Futamura M et al (2011) Pharmacokinetic and pharmacodynamic properties of the glucokinase activator MK-0941 in rodent models of type 2 diabetes and healthy dogs. Mol Pharmacol 80:1156–1165
34. Kendall DM, Cuddihy RM, Bergenstal RM (2009) Clinical application of incretin-based therapy: therapeutic potential, patient selection and clinical use. Am J Med 122:S37–S50
35. Butler AE, Janson J, Bonner-Weir S, Ritzel R, Rizza RA, Butler PC (2003) Beta-cell deficit and increased beta-cell apoptosis in humans with type 2 diabetes. Diabetes 52:102–110

THE JOURNAL OF IMMUNOLOGY

Adiponectin Regulates Cutaneous Wound Healing by Promoting Keratinocyte Proliferation and Migration via the ERK Signaling Pathway

Sayaka Shibata, Yayoi Tada, Yoshihide Asano, Carren S. Hau, Toyoaki Kato, Hidehisa Saeki, Toshimasa Yamauchi, Naoto Kubota, Takashi Kadowaki and Shinichi Sato

J Immunol 2012; 189:3231-3241; Prepublished online 17 August 2012;
doi: 10.4049/jimmunol.1101739
http://www.jimmunol.org/content/189/6/3231

The Journal of Immunology is published twice each month by
The American Association of Immunologists, Inc.,
9650 Rockville Pike, Bethesda, MD 20814-3994.

Print ISSN: 0022-1767 Online ISSN: 1550-6606.

Adiponectin Regulates Cutaneous Wound Healing by Promoting Keratinocyte Proliferation and Migration via the ERK Signaling Pathway

Sayaka Shibata,* Yayoi Tada,* Yoshihide Asano,* Carren S. Hau,* Toyoaki Kato,* Hidehisa Saeki,* Toshimasa Yamauchi,† Naoto Kubota,† Takashi Kadowaki,† and Shinichi Sato*

Diabetic patients are at high risk of developing delayed cutaneous wound healing. Adiponectin plays a pivotal role in the pathogenesis of diabetes and is considered to be involved in various pathological conditions associated with diabetes; however, its role in wound repair is unknown. In this study, we elucidated the involvement of adiponectin in cutaneous wound healing in vitro and in vivo. Normal human keratinocytes expressed adiponectin receptors, and adiponectin enhanced proliferation and migration of keratinocytes in vitro. This proliferative and migratory effect of adiponectin was mediated via AdipoR1/AdipoR2 and the ERK signaling pathway. Consistent with in vitro results, wound closure was significantly delayed in adiponectin-deficient mice compared with wild-type mice, and more importantly, keratinocyte proliferation and migration during wound repair were also impaired in adiponectin-deficient mice. Furthermore, both systemic and topical administration of adiponectin ameliorated impaired wound healing in adiponectin-deficient and diabetic *db/db* mice, respectively. Collectively, these results indicate that adiponectin is a potent mediator in the regulation of cutaneous wound healing. We propose that upregulation of systemic and/or local adiponectin levels is a potential and very promising therapeutic approach for dealing with diabetic wounds. ***The Journal of Immunology*****, 2012, 189: 3231–3241.**

Adipose tissue, located beneath the skin, was initially recognized merely as a site of energy storage. However, increasing evidence indicates that adipose tissue secretes various bioactive molecules and exerts multiple functions in concert with the epidermis and dermis via endo-, para-, and autocrine pathways (1, 2). Adipose tissue is now considered to be a key participant in the development of skin pathophysiology.

Bioactive molecules secreted from adipocytes are termed adipokines. Most adipokines, including TNF-α, IL-6, and resisitin, increase the risk of metabolic syndrome (3). In contrast, another adipokine, adiponectin, ameliorates insulin resistance and mediates antidiabetic effects in liver and skeletal muscle (4, 5). Adiponectin-deficient mice exhibit insulin resistance and glucose intolerance. Administration of adiponectin increases glucose uptake and fat oxidation in muscle, reduces glucose production in liver, and improves insulin sensitivity (6). Thus, adiponectin is a crucial factor in the pathogenesis of diabetes. Adiponectin is present at relatively high concentrations 3–30 μg/ml in circulation, and adiponectin levels are lower in obese and type 2 diabetes patients (7). Accumulated evidence shows that adiponectin is involved in the various pathological conditions associated with diabetes, such as arterial sclerosis, nephropathy, collateral vessel development, and ocular complications (8–10).

Diabetic patients frequently suffer from severely impaired wound healing, with a lifetime risk of 15% for developing diabetic skin ulcerations (11). Diabetic ulcers have a poor prognosis, and 15–27% of all diabetic ulcers lead to the surgical removal of bone (12). However, the mechanisms underlying impaired wound healing in diabetes are poorly understood (13). Wound healing involves a complex biological and molecular cascade of events, including inflammation, granulation tissue formation, re-epithelialization, and angiogenesis (14). Specifically, the re-epithelialization process is critical to optimal wound closure because of its role in wound contraction, which is mediated by keratinocyte proliferation and migration (14). These processes are regulated by the balance of various cytokines, chemokines, and growth factors released by adipose tissue as well as platelets, monocytes, and keratinocytes (1). Adipose tissue participates in cutaneous wound healing as a source of cytokines and growth factors, such as fibroblast growth factors (15), insulin-like growth factor (16), epidermal growth factor (EGF)-like growth factor (17), vascular endothelial growth factor, and angiopoietin-1 (18), and regulates skin wound repair in all layers of the skin via the endocrine/paracrine/autocrine pathways. Indeed, a recent study has shown that adipose tissue extracts, seeded over skin wounds, promotes wound repair (19). Furthermore, leptin, which is another representative adipokine and also secreted from adipocytes, induces keratinocyte proliferation and systemically and topically supplemented leptin improved re-epithelialization of wounds in leptin-deficient *ob/ob* mice and wild-type mice (20, 21).

In this study, to investigate the role of adiponectin during the cutaneous wound healing, we first focused on the functions of keratinocytes, key mediators of the re-epithelialization process, and

*Department of Dermatology, Faculty of Medicine, University of Tokyo, Tokyo 113-8655, Japan; and †Department of Metabolic Diseases, Faculty of Medicine, University of Tokyo, Tokyo 113-8655, Japan

Received for publication June 13, 2011. Accepted for publication July 19, 2012.

This work was supported by Health Science Research grants from the Ministry of Health, Labor and Welfare of Japan and grants from the Ministry of Education, Culture, Sports, Science and Technology-Japan.

Address correspondence and reprint requests to Dr. Yayoi Tada, Department of Dermatology, Faculty of Medicine, University of Tokyo, 7-3-1 Hongo, Bunkyo-ku, Tokyo 113-8655, Japan. E-mail address: ytada-tky@umin.ac.jp

The online version of this article contains supplemental material.

Abbreviations used in this article: AMPK, AMP-activated protein kinase; BHE, bovine hypothalamic extract; EGF, epidermal growth factor; HGF, hepatocyte growth factor; KO, knockout; qrt-PCR, quantitative real-time RT-PCR; siRNA, small interfering RNA.

www.jimmunol.org/cgi/doi/10.4049/jimmunol.1101739

performed functional analyses regarding proliferative and migratory effects. We further examined how adiponectin would be involved in vivo during the wound repair process, using a mouse model of excisional skin wound healing in adiponectin-deficient and diabetic *db/db* mice. The results of this study indicate that adiponectin enhances proliferation and migration of keratinocytes through AdipoR1/AdipoR2 and the ERK signaling pathway in vitro and that adiponectin regulates the skin wound healing process in vivo by promoting keratinocyte proliferation and migration.

Materials and Methods

Reagents

Recombinant human adiponectin was isolated and purified as described previously (22). We verified that purified recombinant adiponectin was free of endotoxin using an endotoxin detection kit (GenScript, Piscataway, NJ). Abs against ERK, p-ERK, p38, p-p38, JNK, p-JNK, Akt, p-Akt, and β-actin were obtained from Cell Signaling Technology (Beverly, MA). Abs against adiponectin, AdipoR1, and AdipoR2 were from Abcam (Cambridge, U.K.). Abs against Ki67 and loricrin were obtained from Novo Castra Laboratories (Newcastle, U.K.) and Covance (Berkeley, CA), respectively. PD98059, U0126, wortmannin, LY294002, SB203580, and SP600125 were also purchased from Cell Signaling Technology.

Cell culture

Normal human epidermal keratinocytes were cultured with MCDB153 medium supplemented with insulin (5 μg/ml), hydrocortisone (1 μM), ethanolamine (0.1 mM), phosphoethanolamine (0.1 mM), bovine hypothalamic extract (BHE) (50 μg/ml), and Ca^{2+} (0.1 mM) as described previously (23, 24). Third or fourth passage cells were used in this study.

RNA interference for adiponectin receptors

All transfections were done using Lipofectamine 2000 following the manufacturer's instructions (Invitrogen Life Technologies, Carlsbad, CA). Keratinocytes were plated in 6-well plates and cultured without antibiotics until reaching 30–50% subconfluency. AdipoR1/AdipoR2/calreticulin/T-cadherin and negative control small interfering RNA (siRNA) (Thermo Scientific Dharmacon, Lafayette, CO) were transfected into keratinocytes using Lipofectamine 2000. Medium was changed after 6 h after trans-

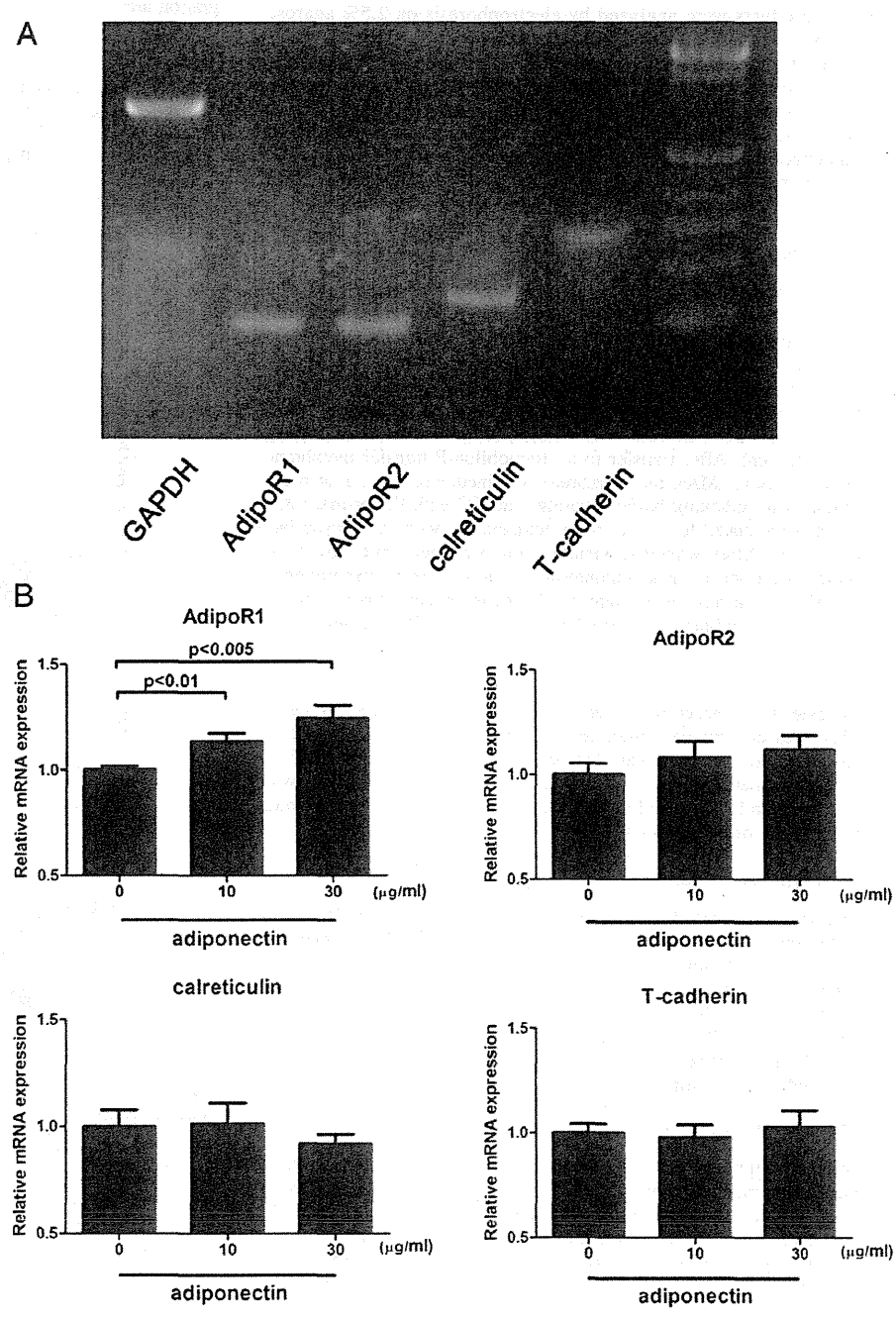

FIGURE 1. Expression of adiponectin receptors in normal human keratinocytes. (A) AdipoR1, AdipoR2, calreticulin, and T-cadherin mRNA expression in cultured primary normal human keratinocytes. Representative data from three independent experiments are shown. (B) Effect of adiponectin on AdipoR1/AdipoR2/calreticulin/T-cadherin mRNA expression in keratinocytes. Normal human keratinocytes were treated with indicated amounts of adiponectin for 9 h, and mRNA expression of AdipoR1/AdipoR2/calreticulin/T-cadherin was examined by qrt-PCR. Data are shown as mean 6 SE (n = 8).

fection, and cells were incubated for another 24 h before subsequent analyses. Gene mRNA expression was examined by real-time RT-PCR analysis.

RT-PCR and quantitative real-time RT-PCR analysis

Total RNA was extracted from cultured keratinocytes and mouse back skin using an RNeasy Mini kit and RNeasy fibrous Tissue Mini kits, respectively (Qiagen, Germantown, MD), respectively. cDNA was synthesized using Superscript III First strand synthesis kits (Invitrogen).

For RT-PCR, synthesized cDNA was thermocycled for PCR amplification with 10 μM of each primer and 1.5 U Taq polymerase (Invitrogen). Primers for amplification, and the sizes of respective PCR products were as follows: AdipoR1, 5′-AATTCCTGAGCGCTTCTTTCCT-3′ and 5′-CATAGAAGTGGACAAAGGCTGC-3′; AdipoR2, 5′-TGCAGCCATTATAGTCTCCCAG-3′ and 5′-GAATGATTCCACTCAGGCCTAG-3′ (25); calreticulin, 5′-AAGTTCTACGGTGACGAGGAG-3′ and 5′-GTCGATGTTCTGCTCATGTTC-3′ (26); T-cadherin, 5′-GCCACGATCATGATCGATGAC-3′ and 5′-GTCTTCATTTTCCACTTTGA-3′ (27); and glyceraldehyde-3-phosphate dehydrogenase gene, 5′-TGAAGGTCGGAGTCAACGGATTTGGT-3′ and 5′-CATGTGGGCCATGAGGTCCACCAC-3′ (28). PCR was performed by 94°C for 5 min, 30 cycles of 94°C for 45 s, 60°C for 45 s, and 72°C for 45 s and a final extension at 72°C for 3 min. The PCR products were analyzed by electrophoresis on 2.5% agarose gels and stained with ethidium bromide, viewed by UV light.

For quantitative real-time RT-PCR (qrt-PCR), gene expression was quantified using TaqMan gene expression assay (Applied Biosystems, Warrington, U.K.). PCR conditions were 95°C for 10 min, 40 cycles of 94°C for 15 s, 60°C for 1 min. All samples were analyzed in parallel for glyceraldehyde-3-phosphate dehydrogenase gene expression as an internal control. The relative change in the levels of genes of interest was determined by the $2^{2\,4\,4\,CT}$ method.

Western blot analysis

Subconfluent keratinocytes were lysed in lysis buffer containing 20 mM Tris (pH 7.5), 150 mM NaCl, 1 mM EDTA, 1 mM EGTA, 1% Triton X-100, 2.5 mM sodium pyrophosphate, 1 mM glycerophosphate, 1 mM sodium orthovanadate, 1 mM PMSF, and 1 μg/ml leupeptin. Samples were dissolved in NuPAGE LDS Sample Buffer with NuPAGE Sample Reducing Agent (Invitrogen) and denatured by heating 5 min at 95°C. SDS-PAGE was performed with NuPAGE 4–12% Bis-Tris gels and MES running buffer (Invitrogen). After transfer to an Immobilon-P transfer membrane (Millipore, Bedford, MA), the membrane was incubated for 1 h at room temperature with blocking buffer, overnight at 4°C with the primary Ab, washed, and incubated for 1 h at room temperature with the appropriate secondary Ab. After washing, visualization was performed by ECL (Amersham Biosciences, Buckinghamshire, U.K.). In some experiments, phospho-ERK1/2 levels were quantified by densitometric analysis using ImageJ (available online) and normalized to the total ERK 1/2 levels.

MTT assay

Keratinocytes were seeded on 12-well plates at a density of 2 3 10^4 cells/well. The next day, the cells were fed MCDB153 medium lacking BHE, and the following day, they were fed once again with the same medium containing designated amounts of adiponectin. After 3 d, cell viability was assessed using an MTT assay kit (Roche Diagnostics, Basel, Switzerland), according to the manufacturer's instructions.

BrdU incorporation assay

Keratinocytes were seeded on 96-well plates at a density of 1 3 10^4 cells/well. After reaching subconfluency, the cells were fed MCDB153 medium lacking BHE. The following day, the cells were fed once again with the same medium containing designated amounts of adiponectin, EGF, and TGF-β and incubated for another 12 h. The cells were then incubated with medium containing BrdU for 2 h. BrdU incorporation was determined using a cell-proliferating ELISA kit (Roche Diagnostics, Basel, Switzerland), according to the manufacturer's instructions.

Boyden chamber assay

Keratinocyte migration was also assayed quantitatively with a Boyden chamber, as described previously (29). Designated amounts of adiponectin and hepatocyte growth factor (HGF) were added to the bottom wells of a 48-well Boyden chamber (Neuro Probe, Gaithersburg, MD), and a 10-μm pore-size polyvinylpyrrolidone-free polycarbonate membrane (Neuro Probe) was placed on the wells. The membrane was precoated with type I collagen (10 μg/ml in PBS; Nitta Gelatin) at room temperature for 1 h and then washed extensively with PBS. Subconfluent keratinocytes were harvested with trypsin–EDTA (0.05% trypsin and 0.5 mM EDTA) and resuspended in culture medium without BHE at 1 3 10^5 cells/ml. A 50-μl aliquot of the keratinocyte suspension (5000 cells/well) was added to the upper wells, and the chamber was incubated overnight at 37°C in a humidified atmosphere of air with 5% CO_2. The cells that adhered to the upper surface of the filter membrane were removed by scraping with a rubber blade, and the cells that moved through the filter and stayed on the lower surface of the membrane were considered to be migrated cells. The membrane was fixed with 10% buffered formalin overnight and then stained with crystal violet. The membrane was then mounted between two glass slides with 90% glycerol, and the number of migrated cells was counted under a microscope.

In vitro wound closure assay

Keratinocytes were seeded on 6-well plates at a density of 1 3 10^5 cells/well. After reaching subconfluency, wounds were created at the center of each well by scraping, and culture debris was removed by PBS washing. The remaining cells were cultured further with designated amounts of adiponectin and HGF. After 12 h, keratinocyte migration was observed under a phase contrast microscope. Wound closure was determined by identifying the front of cell migration and calculating a ratio of the migration area to the area of time 0.

Mice

Adiponectin-deficient mice were generated as described previously (6). BKS.Cg^2 + Lepr db/+ Lepr db (*db/db*) were purchased from CLEA Japan (Tokyo, Japan). Mice were 7- to 10-wk-old for all experiments, and age-matched wild-type C57BL/6 mice (CLEA Japan) were used as controls for adiponectin-deficient and *db/db* mice. All mice were maintained under a 12-h light/12-h dark cycle in a specific pathogen-free barrier facility. All studies and procedures were approved by the Committee on Animal Experimentation of Tokyo University.

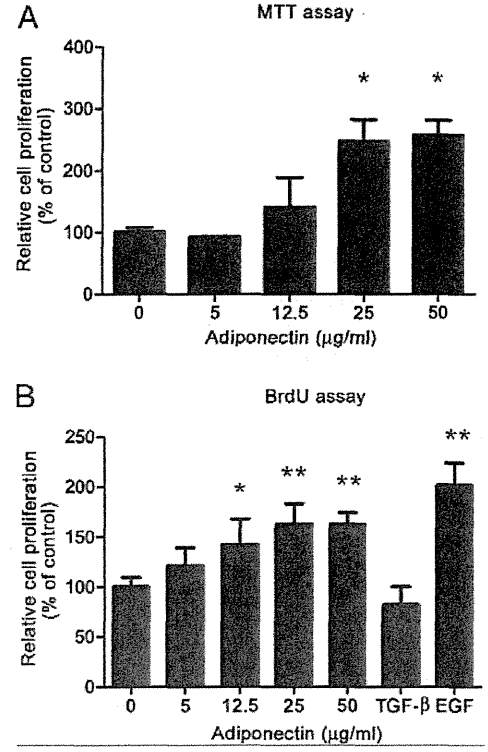

FIGURE 2. Proliferative effects of adiponectin in keratinocytes. (A) After incubation for 3 d with indicated amounts of adiponectin, cell viability was assessed using the MTT assay. Data are shown as mean 6 SE (n = 5) and are representative of four independent experiments. *p , 0.001 versus unstimulated keratinocytes. (B) After incubation for 12 h with indicated amounts of adiponectin, EGF (positive control), and TGF-β (negative control), BrdU incorporation was determined by ELISA. Data are shown as mean 6 SE (n = 8) and are representative of four independent experiments. *p , 0.01, **p , 0.001 versus unstimulated keratinocytes.

Wounding and macroscopic examination

Mice were anesthetized with diethyl ether, and their backs were shaved and wiped with 70% alcohol. Four full-thickness excisional wounds per mouse were made using a disposable sterile 6-mm biopsy punch (Maruho, Osaka, Japan), and mice were caged individually. No signs suggestive of local infection were detected in the wounded skin. We excluded wounds with extreme distortion, which did not permit a precise determination of their size. Areas of open wounds were traced onto a transparency and analyzed using ImageJ (available online).

Histological assessment of wound healing

Skin sections of wounds including a 2-mm rim of unwounded skin tissue were taken from murine back skin. The samples were formalin fixed and embedded in paraffin. Five-micrometer sections were stained with H&E. The epithelial gap, which represents distance between the leading edge of migrating keratinocytes, was measured under a light microscope. For the analyses of staining for adiponectin, AdipoR1/AdipoR2, Ki67, and loricrin, immunohistochemistry was performed using a Vectastain avidin/biotin complex kit (Vector Laboratories, Burlingame, CA), according to the manufacturer's instructions. The 5-μm sections were deparaffinized and rehydrated, endogeneous perioxidase activity was eliminated by blocking with hydrogen peroxide, and the tissue sections were immersed in citrated buffer and boiled for 10 min for Ag retrieval. The sections were then incubated with indicated Abs overnight at 4°C, followed by the incubation with biotinylated secondary Ab. The concentration of each primary Ab was first tested to determine the optimal sensitivity range. The immunoreactivity was visualized with diaminobenzidine, and the sections were counterstained with Mayer's hematoxylin.

Statistical analyses

Data obtained are presented as mean 6 SE. Student *t* test was used for the statistical analysis of differences between two groups. One-way ANOVA with Dunnett's multiple comparison test was used for statistical analysis of the differences among multiple groups. A p value , 0.05 was considered to represent a significant difference.

Results

Adiponectin receptors are expressed in human keratinocytes and AdipoR1 expression is upregulated by adiponectin stimulation

AdipoR1 is expressed widely in various tissues, with the highest expression level in skeletal muscle, whereas AdipoR2 is most abundantly expressed in the liver (30). Recently, new receptors for adiponectin, calreticulin, and T-cadherin also have been identified and reported to be involved in adiponectin cellular signaling (31–34). We first investigated the expressions of these adiponectin receptors in normal human keratinocytes. Human keratinocytes expressed both AdipoR1/AdipoR2 as well as calreticulin and T-cadherin at the mRNA level (Fig. 1A). Adiponectin upregulated gene expression levels of AdipoR1 in a dose-dependent manner but not those of AdipoR2, calreticulin, or T-cadherin in keratinocytes (Fig. 1B).

Adiponectin enhances keratinocyte proliferation

We next investigated the effect of adiponectin on keratinocyte proliferation using the MTT and BrdU assays. The MTT assay quantifies viable cells, whereas the BrdU assay determines BrdU incorporation into newly synthesized DNA of actively proliferating cells. Adiponectin increased the number of viable keratinocytes (Fig. 2A) and BrdU uptake (Fig. 2B) in a dose-dependent manner, reaching a plateau at a concentration of 25 μg/ml. Because plasma adiponectin concentrations in healthy humans are □3–30 μg/ml (36), the stimulatory effects of adiponectin were significant within physiological concentrations. EGF, a positive control, significantly induced keratinocyte proliferation in the BrdU assay, whereas TGF-β, a negative control, had no effect (37).

Adiponectin induces keratinocyte migration

After establishing that adiponectin stimulates keratinocyte proliferation, we next investigated the effect of adiponectin on keratinocyte migration using two types of in vitro assay systems. In the Boyden chamber assay, we quantitatively investigated adiponectin-induced migration. Various amounts of adiponectin and cultured human keratinocytes were added to the lower and upper chambers, respectively. After incubation overnight, the number of migrated cells was counted. Adiponectin significantly stimulated keratinocyte migration at concentrations of 12.5–50 μg/ml (Fig. 3A). HGF was used as a positive control, which induced an □7-fold increase relative to control (38).

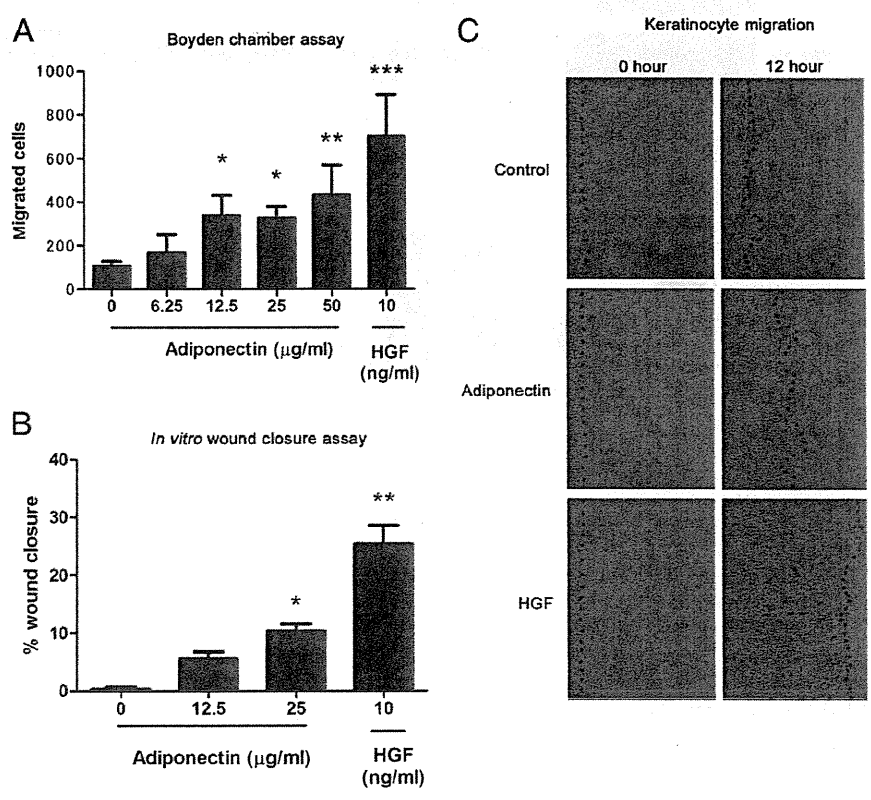

FIGURE 3. Migratory effects of adiponectin in keratinocytes. (A) Keratinocyte migration was assayed quantitatively using the Boyden chamber assay. Indicated amounts of adiponectin and HGF were added to the lower wells. After keratinocytes were added to the upper wells and incubated overnight, the migrated cells were counted. Data are shown as mean 6 SE (n = 6) and are representative of four independent experiments. *p , 0.05, **p , 0.01, ***p , 0.001 versus unstimulated keratinocytes. (B) Keratinocyte migration was assayed using the in vitro wound closure assay. After subconfluent keratinocytes were scraped and incubated with indicated amounts of adiponectin and HGF for 12 h, migration over the wound was measured. Data are shown as mean 6 SE (n = 6) and are representative of three independent experiments. *p , 0.01, **p , 0.001 versus unstimulated keratinocytes. (C) Representative micrograph of keratinocytes directly after (*left panels*) or 12 h after (*right panels*) scraping (original magnification 3 20).

Next, wounds were created in cultured keratinocytes by scraping (in vitro wounds). Keratinocytes were cultured with various concentrations of adiponectin or HGF. Acceleration of wound closure was observed in response to 25 μg/ml adiponectin 12 h after wounding (Fig. 3B, 3C).

The ERK signaling pathway is activated by adiponectin via AdipoR1/AdipoR2 in keratinocytes

MAPK is a well-known factor involved in cell proliferation (39–41). Akt and AMP-activated protein kinase (AMPK) are also known to enhance cell proliferation and suppress apotosis (10). Therefore, we investigated whether adiponectin could induce phosphorylation of MAPKs, Akt and AMPK in normal human keratinocytes. As shown in Fig. 4A, adiponectin (25 μg/ml) induced phosphorylation of ERK in keratinocytes. The peak activation occurred at 5 min after stimulation, and thereafter, the phosphorylation level gradually decreased. Adiponectin had no effect on the phosphorylation of the p38 MAPK, JNK, Akt, and AMPK (Fig. 4B). To confirm the specificity of the identified pathway, keratinocytes were pretreated with 75 μM MEK1 in-

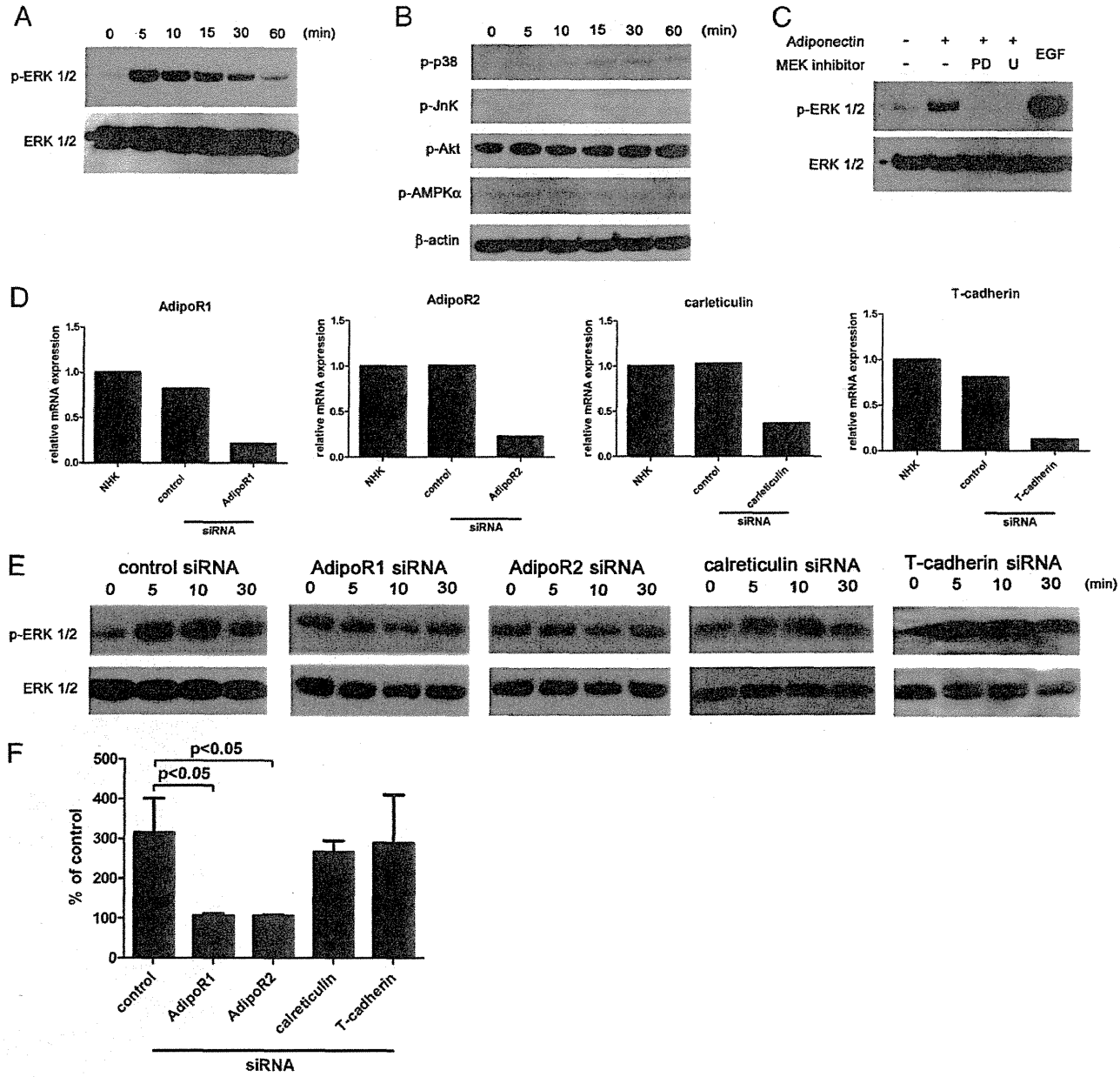

FIGURE 4. Involvement of AdipoR1/AdipoR2 and the ERK signaling pathway in adiponectin-stimulated keratinocytes. (A) Keratinocytes were incubated with adiponectin (25 μg/ml) for 0–60 min. The cell lysates were analyzed for phosphorylation of ERK1/2 by Western blotting. Results are representative of four independent experiments. (B) Keratinocytes were incubated with adiponectin (25 μg/ml) for 0–60 min. The cell lysates were analyzed for phosphorylation of p38 MAPK, JnK, Akt, and AMPK by Western blotting. Results are representative of four independent experiments. (C) Keratinocytes were pretreated with PD98059 (PD; 75 μM, MEK1 inhibitor) or U0126 (U; 10 μM, MEK1/2 inhibitor) for 30 min. After incubation with adiponectin (25 μg/ml) for 5 min, the cell lysates were analyzed for ERK1/2 phosphorylation by Western blotting. Results are representative of four independent experiments. (D) Keratinocytes were transfected with control siRNA or siRNA targeting AdipoR1/AdipoR2/calreticulin/T-cadherin. mRNA expression of these receptors in transfected cells was examined by qrt-PCR. Results are representative of three independent experiments. (E) Transfected cells were incubated with adiponectin (25 μg/ml) for 0–30 min. The cell lysates were analyzed for phosphorylation of ERK1/2 by Western blotting. Results are representative of three independent experiments. (F) Densitometry analysis of P5/P0 (P5, phospho-ERK protein expression levels/total ERK protein expression levels at 5 min after adiponectin stimulation; P0, phospho-ERK protein expression levels/total ERK protein expression levels before adiponectin stimulation), and data are expressed as mean 6 SE ($n = 3$).

hibitor (PD98059) and 10 μM MEK1/2 inhibitor (U0126) for 30 min and then stimulated with adiponectin for 5 min. Both of these inhibitors blocked adiponectin-induced ERK phosphorylation (Fig. 4C). To determine whether the activation of the ERK signaling pathway by adiponectin is mediated through AdipoR1/AdipoR2/calreticulin/T-cadherin, keratinocytes were transfected with siRNAs of these receptors, and specific inhibition was performed. Control experiments have revealed that AdipoR1/AdipoR2/calreticulin/T-cadherin mRNA levels are reduced by . 80% as evaluated by real-time RT-PCR analysis (Fig. 4D). Under these experimental conditions, inhibition of AdipoR1 or AdipoR2 completely suppressed adiponectin-induced ERK phosphorylation in keratinocytes (Fig. 4E, 4F). However, downregulation of calreticulin or T-cadherin did not significantly suppress adiponectin-induced ERK phosphorylation. These results indicate that 1) adiponectin activates the ERK signaling pathway through AdipoR1 and AdipoR2 and that 2) calreticulin or T-cadherin appear not to be involved in the ERK signaling pathway mediated by adiponectin in keratinocytes.

ERK signaling pathway mediates adiponectin-induced keratinocyte proliferation and migration

To investigate the role of the ERK signaling pathway in keratinocyte proliferation induced by adiponectin, we incubated keratinocytes with PD98059 (75 μM) or U0126 (10 μM) for 30 min before stimulation with adiponectin (25 μg/ml), and then, BrdU uptake was analyzed. Both of these inhibitors attenuated BrdU uptake induced by adiponectin, indicating that adiponectin-induced keratinocyte proliferation is mediated by the ERK pathway (Fig. 5A). Other kinase inhibitors (wortmannin and LY294002 for inhibition of PI3K, SB203580 for inhibition of p38 MAPK, and SP600125 for inhibition of JNK) did not affect adiponectin-induced proliferation. We further investigated whether the ERK signaling pathway would be involved in the keratinocyte migration induced by adiponectin. After the addition of PD98059 (75 μM) or U0126 (10 μM) to the lower chamber with adiponectin, keratinocyte migration was analyzed using the Boyden chamber assay. Both of the inhibitors blocked adiponectin-induced keratinocyte migration (Fig. 5B). These results suggest that the ERK signaling pathway mediated adiponectin-induced keratinocyte migration as well as proliferation.

Wound closure and keratinocyte re-epithelialization are significantly delayed in adiponectin-deficient mice

To further strengthen our in vitro results and to determine the role of adiponectin during cutaneous wound healing in vivo, we first examined the excisional wound skin repair process in adiponectin-deficient and wild-type mice. Full-thickness round wounds of 6 mm in diameter were made, and the kinetics of wound closure were evaluated as percentage of original wound areas. Adiponectin-deficient mice exhibited significantly impaired wound repair compared with wild-type mice from day 3 (Fig. 6A, 6B). All the wounds of wild-type mice healed within 9 d after wounding, whereas the wounds of adiponectin-deficient mice took more than 13 d to heal. Next, we focused on the re-epithelialization phase of wound healing, which involves keratinocyte proliferation and migration for wound contraction. To confirm the pattern of keratinocyte differentiation to be normal in the adiponectin-deficient mice skin, we first examined the expression of loricrin, a marker of late-phase keratinocyte differentiation, by immunohistochemistry. Loricrin expression in the keratinocytes was comparable between wild-type and adiponectin-deficient mice (Fig. 6C). Next, we performed immunohistochemistry for the proliferation marker

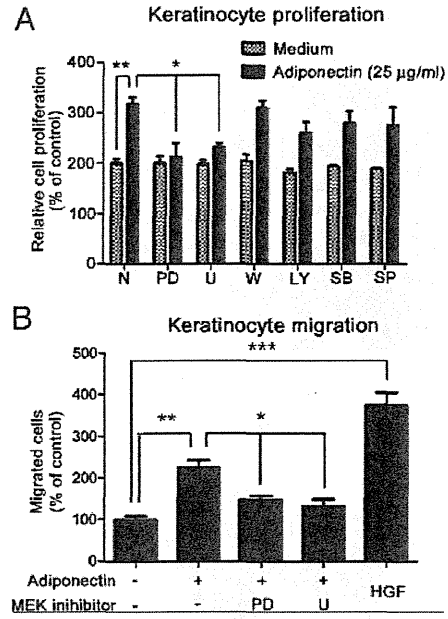

FIGURE 5. Involvement of the ERK signaling pathway in adiponectin-induced proliferation and migration of keratinocytes. (A) Keratinocytes were preincubated with PD98059 (PD; 75 μM), U0126 (U; 10 μM), wortmannin (W; 0.5 μM, PI3K inhibitor), LY294002 (LY; 10 μM, PI3K inhibitor), SB203580 (SB; 10 μM, p38 MAPK inhibitor), and SP600125 (SP; 10 μM, JNK inhibitor) or without inhibitors (N). After incubation with adiponectin for 12 h, keratinocyte proliferation was analyzed using the BrdU assay. Data are shown as mean 6 SE (n = 8) and are representative of four independent experiments. *p , 0.05 versus medium treated with adiponectin (25 μg/ml), **p , 0.001 versus medium alone. (B) Indicated amounts of adiponectin with or without PD98059 (PD; 75 μM) and U0126 (U; 10 μM) were added to the lower wells. Keratinocyte migration was analyzed using the Boyden chamber assay. Data are shown as mean 6 SE (n = 6) and are representative of three independent experiments. *p , 0.05 versus medium treated with adiponectin (25 μg/ml), **p , 0.01 and ***p , 0.001 versus medium alone.

Ki67 on the skin samples of the wound margins (20, 42). Distribution of Ki67-positive proliferating keratinocytes was more intensive in the wound margins of control wild-type mice compared with adiponectin knockout (KO) mice (Fig. 6D, 6E). Furthermore, the epithelial gap, the distance between the migrating edges of keratinocytes, was significantly wider in adiponectin-deficient mice compared with wild-type mice (Fig. 6A, 6F), suggesting that keratinocyte migration was significantly inhibited in adiponectin-deficient mice. These results are in accordance with the in vitro results regarding the proliferative and migratory functions of adiponectin in keratinocytes.

The gene expression of adiponectin and AdipoR1/AdipoR2 gradually increases during the wound healing process

To determine whether the local adiponectin and AdipoR1/AdipoR2 expression levels change during the wound healing process, we determined the changes in expression of these genes over time. Skin samples, taken immediately before (at day 0) and 3 and 6 d (days 3 and 6) after wounding, were analyzed by the qrt-PCR. We demonstrate in this study that adiponectin expression at the wound site gradually increased during the course of wound repair in wild-type mice (Fig. 7A), suggesting that adiponectin production might be upregulated sensing tissue damage of wounding. Immunohistochemistry of adiponectin showed that the sources of adiponectin are adipocytes and fibroblasts but not keratinocytes (Fig. 7B). Regarding adiponectin receptors, AdipoR1 and AdipoR2 mRNA expression also increased gradually after wounding in both wild-

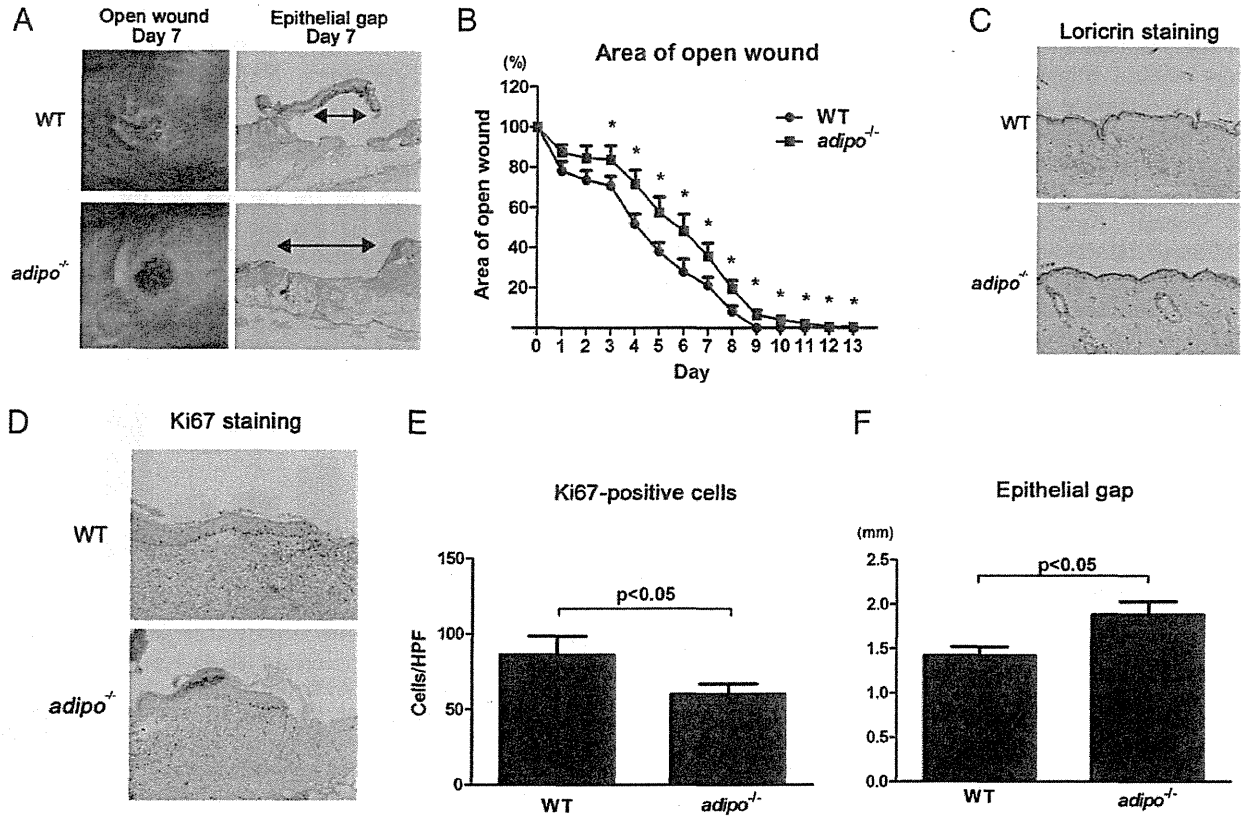

FIGURE 6. The kinetics of wound closure and evaluation of proliferative and migratory properties in adiponectin-deficient and wild-type mice. (A) Representative photographs of open wounds at day 7 and histology of the epithelial gap in wild-type and adiponectin-deficient mice (original magnification 3 40). In histological sections, the edges of keratinocytes are indicated by arrows. (B) Area of open wound in wild-type and adiponectin-deficient mice was evaluated daily. Fifty wounds from 16 wild-type and 45 wounds from 14 adiponectin-deficient mice were used for the analysis. Data are shown as mean 6 SE. (C) Immunohistochemistry of loricrin in the skin sections taken before wounding of wild-type and adiponectin-deficient mice (original magnification 3 400). (D) Immunohistochemistry of Ki-67 in the skin sections taken 3 d after wounding of wild-type and adiponectin-deficient mice (original magnification 3 200). (E) The number of Ki67-positive cells in keratinocytes of the wound margins 3 d after wounding. Ki67-positive cells were counted in high-power field (HPF) from 10 wounds ($n = 4$ mice/group). Data are shown as mean 6 SE. (F) The epithelial gap was microscopically measured in the skin sections taken 7 d after wounding of wild-type and adiponectin-deficient mice. Thirteen wounds from six wild-type and 10 wounds from four adiponectin-deficient mice were used for the analysis. Data are shown as mean 6 SE.

type and adiponectin KO mice (Fig. 7C). The expression levels of these receptors during wound repair were comparable between wild-type and adiponectin KO mice. We also analyzed AdipoR1 and AdipoR2 expression on cells in wound samples of wild-type and adiponectin KO mice by immunohistochemistry. Protein expression of AdipoR1 and AdipoR2 was detected in fibroblasts and adipocytes as well as keratinocytes, and their expression was upregulated after wounding (Fig. 7D). Taken together, adiponectin, locally produced by adipocytes after skin damage, might induce the upregulation of AdipoR1 and AdipoR2 expression on keratinocytes. This process would further enhance adiponectin-mediated signaling within keratinocytes, thus promoting keratinocyte proliferation and migration.

Systemically supplemented adiponectin ameliorates delayed wound healing in adiponectin-deficient mice but not in wild-type mice

To determine whether the impaired wound healing in adiponectin-deficient mice is particularly adiponectin dependent or not, wild-type and adiponectin-deficient mice were given daily i.p. injection of recombinant adiponectin (50 μg/day/mouse) from 1 d before wounding, and the wound repair process was examined. As shown in Fig. 8A, systemic injection of physiological dose of adiponectin significantly ameliorated impaired wound healing in adiponectin-deficient mice but not in wild-type mice at days 3 and 7. These results may indicate that adiponectin supplementation is effective only under the condition when adiponectin is insufficient.

Topically supplemented adiponectin accelerates delayed wound healing in db/db *mice but not in wild-type mice*

To evaluate a potential clinical application of adiponectin, we investigated whether adiponectin would also act directly at the wound site by administering adiponectin to wound beds directly in *db/db* mice, a rodent model for type 2 diabetes, and wild-type mice. We applied 2.5 μg adiponectin in 50 μl PBS on the left side of the murine back and the same dose of PBS on the right side under the occlusive dressing every day. *db/db* mice were previously shown to have decreased adiponectin levels and impaired wound healing (43). Topical adiponectin administration significantly reduced open wound area relative to PBS administration at days 13, 16, and 19 (Fig. 8B) in *db/db* mice. Re-epithelialization was also assessed at day 13 microscopically, and the epithelial gap was significantly shorter in adiponectin-treated mice relative to PBS-treated mice (Fig. 8C). In contrast, there was no significant difference between adiponectin- and PBS-applied wound areas in wild-type mice (Fig. 8D). These results, as in the case with systemic supplementation, suggest that wound treatment with topical adiponectin is effective in mice with low adiponectin levels (*db/db* mice) but not in mice with normal adiponectin levels (wild-type mice).

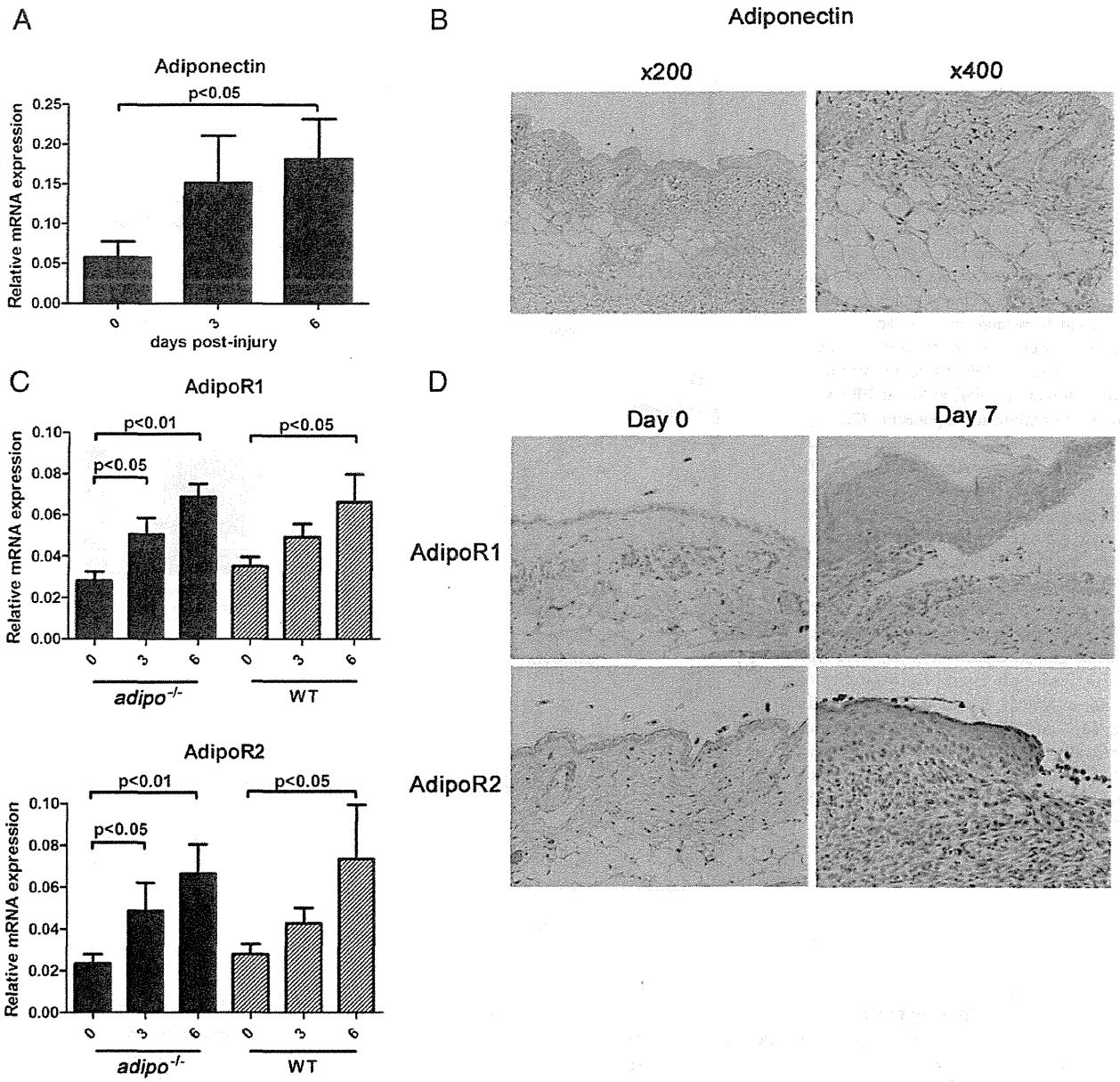

FIGURE 7. Regulation of adiponectin and AdipoR1/AdipoR2 mRNA expression during wound repair. Skin samples were taken immediately before (at day 0) and 3 and 6 d (days 3 and 6) after wounding from wild-type and adiponectin-deficient mice. Gene expression levels of adiponectin (A) and AdipoR1/ AdipoR2 (C) were analyzed by the qrt-PCR. Immunohistochemistry for adiponectin (B) at day 7 in wild-type mice and AdipoR1/ AdipoR2 (D) at days 0 and 7 in wild-type and adiponectin-deficient mice was performed (original magnification 3 400).

Discussion

Adiponectin, a key mediator in the pathogenesis of diabetes, exerts multiple biological activities in various diseases; however, its role in cutaneous wound healing is unknown. To clarify this, we investigated pathophysiologic roles of adiponectin during cutaneous wound healing. We first demonstrated that keratinocytes express adiponectin receptors and that adiponectin induces proliferation and migration of keratinocytes in a dose-dependent manner through ERK activation in vitro. By using siRNAs of adiponectin receptors on keratinocytes, we also determined that AdipoR1 and AdipoR2 are mainly involved in the adiponectin-mediated ERK signaling pathway. These in vitro results suggest that adiponetin might contribute to the re-epithelialization phase of optimal wound healing. We have next undertaken a detailed functional analysis of adiponectin during wound repair in vivo. Wound closure was significantly delayed in adiponectin-deficient mice compared with wild-type mice. The number of Ki67-positive cells in the wound margin epithelial cells was decreased and re-epithelialization was delayed in adiponectin-deficient mice, which were supportive of in vitro results. The expression of AdipoR1/AdipoR2 as well as adiponectin gradually increased after wounding, which may consequently augment adiponectin signaling within keratinocytes and facilitate wound repair. Finally, we examined the curative effect of adiponectin on wounds. Both systemic and topical adiponectin supplementation normalized the impaired wound healing in adiponectin-deficient mice and *db/db* mice, respectively. Thus, adiponectin might contribute to optimal cutaneous wound healing in diabetic patients, whose adiponectin levels are persistently decreased.

With regard to cell proliferation and migration, the behavior of adiponectin seems to depend on cell types. For instance, adiponectin stimulates cell growth in colonic epithelial cells (39), osteoblasts (40), and cardiac fibroblasts (41), where adiponectin is involved in the gastrointenstinal mucosal metabolism, bone me-

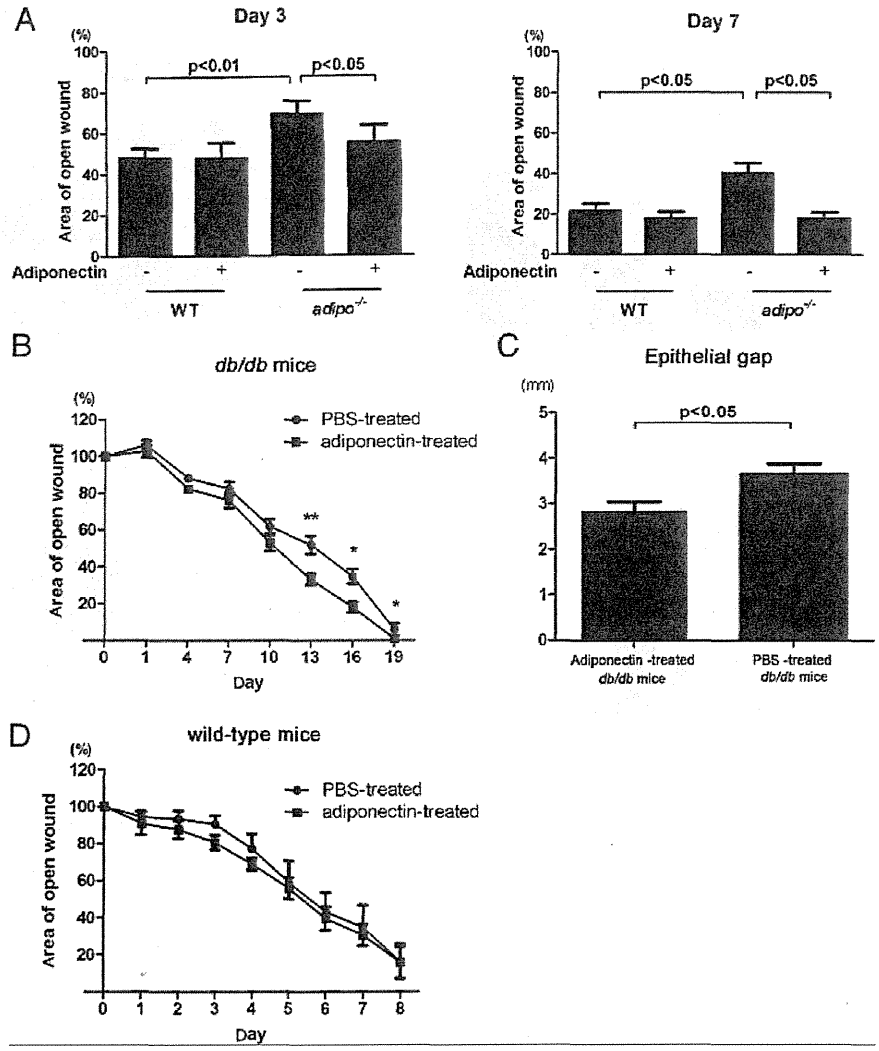

FIGURE 8. Effect of systemically and topically supplemented adiponectin on wound healing in wild-type, adiponectin-deficient, and *db/db* mice. (A) Wild-type and adiponectin-deficient mice were given daily i.p. injection of recombinant adiponectin (50 μg/day), and the area of open wound was measured at days 3 and 7 after wounding. Thirteen wounds from six wild-type and 14 wounds from six adiponectin-deficient mice were used for the analysis. Data are shown as mean 6 SE. (B) *db/db* mice were given daily topical administration of PBS with or without recombinant adiponectin (2.5 μg/day), and the area of open wound was measured after wounding. Data are shown as mean 6 SE, obtained from five *db/db* mice (10 wounds for adiponectin-treated and PBS-treated group, respectively). (C) The epithelial gap was microscopically measured in the skin sections taken 13 d after wounding of *db/db* mice. Data are shown as mean 6 SE, obtained from five *db/db* mice (10 wounds for adiponectin-treated and PBS-treated group, respectively). (D) Wild-type mice were given daily topical administration of PBS with or without recombinant adiponectin (2.5 μg/day), and the area of open wound was measured after wounding. Data are shown as mean 6 SE, obtained from five wild-type mice (10 wounds for adiponectin-treated and PBS-treated group, respectively).

tabolism, and myocardial hypertrophy, respectively. Migratory effects of adiponectin have been reported in endothelial progenitor cells (44). In contrast, adiponectin suppressed cell proliferation and migration in vascular smooth muscle cells (45) and hepatic stellate cells (46), acting as a modulator for vascular remodeling and liver fibrosis, respectively. Most importantly, a certain subset of cell types that are involved in the cutaneous wound healing process exhibit proliferative and migratory behaviors in response to adiponectin. Dermal fibroblasts are the dominant players in the process of granulation tissue formation during cutaneous wound healing. Recent reports have revealed that adiponectin induces proliferation of dermal fibroblasts and upregulation of collagen production (47, 48). Furthermore, adiponectin induces proliferation of HUVECs and stimulates angiogenesis (10), indicating the positive contribution of adiponectin to optimal wound repair. In addition, adiponectin induces neutrophil migration, which is an initial step of skin wound repair (14). In this study, adiponectin exhibited proliferative and migratory effects on primary human keratinocytes. Proliferation and migration of keratinocytes are crucial factors of re-epithelialization, which marks the final stage of wound healing (14). Given that inflammation, granulation tissue formation, re-epithelialization, and angiogenesis are sequential central events, adiponectin may play a vital role throughout the wound healing process. It should be mentioned that Kawai et al. (49) previously reported that adiponectin slightly suppressed the proliferation of the immortalized keratinocyte cell line HaCaT. Therefore, we also investigated whether adiponectin would exert effects on HaCaT cells as well; however, in our hands, adiponectin had no effect on proliferation of these cells (Supplemental Fig. 1). Although the reason for the discrepancy of the results between primary normal human keratinocytes and HaCaT cells is not clear, HaCaT cells have been reported to behave differently from normal human keratinocytes regarding cell growth, differentiation, and cytokine production in several reports (50, 51).

Consistent with our in vitro results, a significant impairment of wound repair was also observed in adiponectin-deficient mice in the current study. Furthermore, both systemic and topical adiponcetin accelerated wound repair in adiponectin-deficient and diabetic *db/db* mice, respectively. In contrast, the wound closure rate of wild-type mice did not change after systemic or local administration of adiponectin. Thus, adiponectin has beneficial and direct effects on cutaneous wound healing, especially in diabetic patients whose adiponectin levels are constitutively decreased. These findings would suggest that upregulating serum adiponectin levels through medical treatment as well as raising cutaneous local adiponectin levels by direct administration of adiponectin to the wound sites represents a novel effective therapeutic target for delayed diabetic wounds (52).

There has been no information available regarding the adiponectin-induced intracellular signaling in keratinocytes. The signaling pathways involved in cell proliferation and migration by adiponectin are tissue-/cell type-specific, including p38 MAPK,

JNK, ERK, PI3K, and Akt (10, 39–41). In the current study, we demonstrate that the proliferative and migratory activities of adiponectin are mediated through ERK signaling. It has been reported that the ERK signaling pathway is activated as a downstream signal molecule of adiponectin receptors in several cell types, including endothelial cells, macrophages, cardiac fibroblasts, and pancreatic cells (10, 41, 53, 54). Previous studies have shown that the ERK signaling pathway is activated upon injury or stretching of keratinocytes (55, 56). Interestingly, ERK pathways are required for wound healing in corneal epithelial cells under high glucose conditions (57). Considering that ERK activation is required for keratinocyte proliferation and migration (58), our present result showing that adiponectin activates the ERK signaling pathway in keratinocytes would suggest that adiponectin positively regulates the re-epithelialization process during cutaneous wound healing.

In summary, we propose a potent role for adiponectin, a key mediator of diabetes, in the regulation of keratinocyte proliferation and migration during cutaneous wound healing and provide a new mechanism underlying delayed wound repair in diabetic patients. On the basis of our data, we propose that systemic and/or local upregulation of adiponectin levels may represent a novel therapeutic strategy for diabetic wounds.

Acknowledgments

We thank Dr. Wolfgang W. Leitner (National Institute of Allergy and Infectious Diseases, National Institutes of Health) for helpful discussions.

Disclosures

The authors have no financial conflicts of interest.

References

1. Klein, J., P. A. Permana, M. Owecki, G. N. Chaldakov, M. Böhm, G. Hausman, C. M. Lapière, P. Atanassova, J. Sowiński, M. Fasshauer, et al. 2007. What are subcutaneous adipocytes really good for? *Exp. Dermatol.* 16: 45–70.
2. Scherer, P. E. 2006. Adipose tissue: from lipid storage compartment to endocrine organ. *Diabetes* 55: 1537–1545.
3. Kadowaki, T., T. Yamauchi, and N. Kubota. 2008. The physiological and pathophysiological role of adiponectin and adiponectin receptors in the peripheral tissues and CNS. *FEBS Lett.* 582: 74–80.
4. Yamauchi, T., J. Kamon, Y. Minokoshi, Y. Ito, H. Waki, S. Uchida, S. Yamashita, M. Noda, S. Kita, K. Ueki, et al. 2002. Adiponectin stimulates glucose utilization and fatty-acid oxidation by activating AMP-activated protein kinase. *Nat. Med.* 8: 1288–1295.
5. Kadowaki, T., T. Yamauchi, N. Kubota, K. Hara, K. Ueki, and K. Tobe. 2006. Adiponectin and adiponectin receptors in insulin resistance, diabetes, and the metabolic syndrome. *J. Clin. Invest.* 116: 1784–1792.
6. Kubota, N., Y. Terauchi, T. Yamauchi, T. Kubota, M. Moroi, J. Matsui, K. Eto, T. Yamashita, J. Kamon, H. Satoh, et al. 2002. Disruption of adiponectin causes insulin resistance and neointimal formation. *J. Biol. Chem.* 277: 25863–25866.
7. Hotta, K., T. Funahashi, Y. Arita, M. Takahashi, M. Matsuda, Y. Okamoto, H. Iwahashi, H. Kuriyama, N. Ouchi, K. Maeda, et al. 2000. Plasma concentrations of a novel, adipose-specific protein, adiponectin, in type 2 diabetic patients. *Arterioscler. Thromb. Vasc. Biol.* 20: 1595–1599.
8. Shibata, R., K. Sato, M. Kumada, Y. Izumiya, M. Sonoda, S. Kihara, N. Ouchi, and K. Walsh. 2007. Adiponectin accumulates in myocardial tissue that has been damaged by ischemia-reperfusion injury via leakage from the vascular compartment. *Cardiovasc. Res.* 74: 471–479.
9. Ohashi, K., H. Iwatani, S. Kihara, Y. Nakagawa, N. Komura, K. Fujita, N. Maeda, M. Nishida, F. Katsube, I. Shimomura, et al. 2007. Exacerbation of albuminuria and renal fibrosis in subtotal renal ablation model of adiponectin-knockout mice. *Arterioscler. Thromb. Vasc. Biol.* 27: 1910–1917.
10. Ouchi, N., H. Kobayashi, S. Kihara, M. Kumada, K. Sato, T. Inoue, T. Funahashi, and K. Walsh. 2004. Adiponectin stimulates angiogenesis by promoting cross-talk between AMP-activated protein kinase and Akt signaling in endothelial cells. *J. Biol. Chem.* 279: 1304–1309.
11. Jeffcoate, W. J., and K. G. Harding. 2003. Diabetic foot ulcers. *Lancet* 361: 1545–1551.
12. Kämpfer, H., R. Schmidt, G. Geisslinger, J. Pfeilschifter, and S. Frank. 2005. Wound inflammation in diabetic ob/ob mice: functional coupling of prostaglandin biosynthesis to cyclooxygenase-1 activity in diabetes-impaired wound healing. *Diabetes* 54: 1543–1551.
13. Falanga, V. 2005. Wound healing and its impairment in the diabetic foot. *Lancet* 366: 1736–1743.
14. Singer, A. J., and R. A. Clark. 1999. Cutaneous wound healing. *N. Engl. J. Med.* 341: 738–746.
15. Yamashita, H., S. Oh-ishi, T. Kizaki, J. Nagasawa, D. Saitoh, Y. Ohira, and H. Ohno. 1995. Insulin stimulates the expression of basic fibroblast growth factor in rat brown adipocyte primary culture. *Eur. J. Cell Biol.* 68: 8–13.
16. Zizola, C. F., M. E. Balañá, M. Sandoval, and J. C. Calvo. 2002. Changes in IGF-I receptor and IGF-I mRNA during differentiation of 3T3-L1 preadipocytes. *Biochimie* 84: 975–980.
17. Matsuzawa, Y. 2006. The metabolic syndrome and adipocytokines. *FEBS Lett.* 580: 2917–2921.
18. Kosacka, J., M. Nowicki, J. Kacza, J. Borlak, J. Engele, and K. Spanel-Borowski. 2006. Adipocyte-derived angiopoietin-1 supports neurite outgrowth and synaptogenesis of sensory neurons. *J. Neurosci. Res.* 83: 1160–1169.
19. Fu, X., L. Fang, H. Li, X. Li, B. Cheng, and Z. Sheng. 2007. Adipose tissue extract enhances skin wound healing. *Wound Repair Regen.* 15: 540–548.
20. Frank, S., B. Stallmeyer, H. Kämpfer, N. Kolb, and J. Pfeilschifter. 2000. Leptin enhances wound re-epithelialization and constitutes a direct function of leptin in skin repair. *J. Clin. Invest.* 106: 501–509.
21. Stallmeyer, B., H. Kämpfer, M. Podda, R. Kaufmann, J. Pfeilschifter, and S. Frank. 2001. A novel keratinocyte mitogen: regulation of leptin and its functional receptor in skin repair. *J. Invest. Dermatol.* 117: 98–105.
22. Yamauchi, T., J. Kamon, H. Waki, Y. Terauchi, N. Kubota, K. Hara, Y. Mori, T. Ide, K. Murakami, N. Tsuboyama-Kasaoka, et al. 2001. The fat-derived hormone adiponectin reverses insulin resistance associated with both lipoatrophy and obesity. *Nat. Med.* 7: 941–946.
23. Shirakata, Y., T. Komurasaki, H. Toyoda, Y. Hanakawa, K. Yamasaki, S. Tokumaru, K. Sayama, and K. Hashimoto. 2000. Epiregulin, a novel member of the epidermal growth factor family, is an autocrine growth factor in normal human keratinocytes. *J. Biol. Chem.* 275: 5748–5753.
24. Shibata, S., Y. Tada, N. Kanda, K. Nashiro, M. Kamata, M. Karakawa, T. Miyagaki, H. Kai, H. Saeki, Y. Shirakata, et al. 2010. Possible roles of IL-27 in the pathogenesis of psoriasis. *J. Invest. Dermatol.* 130: 1034–1039.
25. Takahata, C., Y. Miyoshi, N. Irahara, T. Taguchi, Y. Tamaki, and S. Noguchi. 2007. Demonstration of adiponectin receptors 1 and 2 mRNA expression in human breast cancer cells. *Cancer Lett.* 250: 229–236.
26. Taguchi, J., A. Fujii, Y. Fujino, Y. Tsujioka, M. Takahashi, Y. Tsuboi, I. Wada, and T. Yamada. 2000. Different expression of calreticulin and immunoglobulin binding protein in Alzheimer's disease brain. *Acta Neuropathol.* 100: 153–160.
27. Takeuchi, T., S. B. Liang, N. Matsuyoshi, S. Zhou, Y. Miyachi, H. Sonobe, and Y. Ohtsuki. 2002. Loss of T-cadherin (CDH13, H-cadherin) expression in cutaneous squamous cell carcinoma. *Lab. Invest.* 82: 1023–1029.
28. Fujimoto, S., H. Uratsuji, H. Saeki, S. Kagami, Y. Tsunemi, M. Komine, and K. Tamaki. 2008. CCR4 and CCR10 are expressed on epidermal keratinocytes and are involved in cutaneous immune reaction. *Cytokine* 44: 172–178.
29. Boyden, S. 1962. The chemotactic effect of mixtures of antibody and antigen on polymorphonuclear leucocytes. *J. Exp. Med.* 115: 453–466.
30. Yamauchi, T., J. Kamon, Y. Ito, A. Tsuchida, T. Yokomizo, S. Kita, T. Sugiyama, M. Miyagishi, K. Hara, M. Tsunoda, et al. 2003. Cloning of adiponectin receptors that mediate antidiabetic metabolic effects. *Nature* 423: 762–769.
31. Denzel, M. S., M. C. Scimia, P. M. Zumstein, K. Walsh, P. Ruiz-Lozano, and B. Ranscht. 2010. T-cadherin is critical for adiponectin-mediated cardioprotection in mice. *J. Clin. Invest.* 120: 4342–4352.
32. Lee, M. H., R. L. Klein, H. M. El-Shewy, D. K. Luttrell, and L. M. Luttrell. 2008. The adiponectin receptors AdipoR1 and AdipoR2 activate ERK1/2 through a Src/Ras-dependent pathway and stimulate cell growth. *Biochemistry* 47: 11682–11692.
33. Maruyama, S., R. Shibata, K. Ohashi, T. Ohashi, H. Daida, K. Walsh, T. Murohara, and N. Ouchi. 2011. Adiponectin ameliorates doxorubicin-induced cardiotoxicity through Akt protein-dependent mechanism. *J. Biol. Chem.* 286: 32790–32800.
34. Ohashi, K., N. Ouchi, K. Sato, A. Higuchi, T. O. Ishikawa, H. R. Herschman, S. Kihara, and K. Walsh. 2009. Adiponectin promotes revascularization of ischemic muscle through a cyclooxygenase 2-dependent mechanism. *Mol. Cell. Biol.* 29: 3487–3499.
35. Ouchi, N., and K. Walsh. 2008. A novel role for adiponectin in the regulation of inflammation. *Arterioscler. Thromb. Vasc. Biol.* 28: 1219–1221.
36. Kelesidis, I., T. Kelesidis, and C. S. Mantzoros. 2006. Adiponectin and cancer: a systematic review. *Br. J. Cancer* 94: 1221–1225.
37. Wenczak, B. A., J. B. Lynch, and L. B. Nanney. 1992. Epidermal growth factor receptor distribution in burn wounds: implications for growth factor-mediated repair. *J. Clin. Invest.* 90: 2392–2401.
38. Matsumoto, K., K. Hashimoto, K. Yoshikawa, and T. Nakamura. 1991. Marked stimulation of growth and motility of human keratinocytes by hepatocyte growth factor. *Exp. Cell Res.* 196: 114–120.
39. Ogunwobi, O. O., and I. L. Beales. 2006. Adiponectin stimulates proliferation and cytokine secretion in colonic epithelial cells. *Regul. Pept.* 134: 105–113.
40. Luo, X. H., L. J. Guo, L. Q. Yuan, H. Xie, H. D. Zhou, X. P. Wu, and E. Y. Liao. 2005. Adiponectin stimulates human osteoblasts proliferation and differentiation via the MAPK signaling pathway. *Exp. Cell Res.* 309: 99–109.
41. Hattori, Y., S. Hattori, K. Akimoto, T. Nishikimi, K. Suzuki, H. Matsuoka, and K. Kasai. 2007. Globular adiponectin activates nuclear factor-κB and activating protein-1 and enhances angiotensin II-induced proliferation in cardiac fibroblasts. *Diabetes* 56: 804–808.
42. Gerdes, J., H. Lemke, H. Baisch, H. H. Wacker, U. Schwab, and H. Stein. 1984. Cell cycle analysis of a cell proliferation-associated human nuclear antigen defined by the monoclonal antibody Ki-67. *J. Immunol.* 133: 1710–1715.

43. Tsuboi, R., and D. B. Rifkin. 1990. Recombinant basic fibroblast growth factor stimulates wound healing in healing-impaired db/db mice. *J. Exp. Med.* 172: 245–251.
44. Nakamura, N., K. Naruse, T. Matsuki, Y. Hamada, E. Nakashima, H. Kamiya, T. Matsubara, A. Enomoto, M. Takahashi, Y. Oiso, and J. Nakamura. 2009. Adiponectin promotes migration activities of endothelial progenitor cells via Cdc42/Rac1. *FEBS Lett.* 583: 2457–2463.
45. Arita, Y., S. Kihara, N. Ouchi, K. Maeda, H. Kuriyama, Y. Okamoto, M. Kumada, K. Hotta, M. Nishida, M. Takahashi, et al. 2002. Adipocyte-derived plasma protein adiponectin acts as a platelet-derived growth factor-BB-binding protein and regulates growth factor-induced common postreceptor signal in vascular smooth muscle cell. *Circulation* 105: 2893–2898.
46. Kamada, Y., S. Tamura, S. Kiso, H. Matsumoto, Y. Saji, Y. Yoshida, K. Fukui, N. Maeda, H. Nishizawa, H. Nagaretani, et al. 2003. Enhanced carbon tetrachloride-induced liver fibrosis in mice lacking adiponectin. *Gastroenterology* 125: 1796–1807.
47. Ezure, T., and S. Amano. 2007. Adiponectin and leptin up-regulate extracellular matrix production by dermal fibroblasts. *Biofactors* 31: 229–236.
48. Fu, Y., N. Luo, R. L. Klein, and W. T. Garvey. 2005. Adiponectin promotes adipocyte differentiation, insulin sensitivity, and lipid accumulation. *J. Lipid Res.* 46: 1369–1379.
49. Kawai, K., A. Kageyama, T. Tsumano, S. Nishimoto, K. Fukuda, S. Yokoyama, T. Oguma, K. Fujita, S. Yoshimoto, A. Yanai, and M. Kakibuchi. 2008. Effects of adiponectin on growth and differentiation of human keratinocytes—implication of impaired wound healing in diabetes. *Biochem. Biophys. Res. Commun.* 374: 269–273.
50. Breitkreutz, D., H. J. Stark, P. Plein, M. Baur, and N. E. Fusenig. 1993. Differential modulation of epidermal keratinization in immortalized (HaCaT) and tumorigenic human skin keratinocytes (HaCaT-ras) by retinoic acid and extracellular Ca^{2+}. *Differentiation* 54: 201–217.
51. Tsuda, T., M. Tohyama, K. Yamasaki, Y. Shirakata, Y. Yahata, S. Tokumaru, K. Sayama, and K. Hashimoto. 2003. Lack of evidence for TARC/CCL17 production by normal human keratinocytes in vitro. *J. Dermatol. Sci.* 31: 37–42.
52. Hirose, H., T. Kawai, Y. Yamamoto, M. Taniyama, M. Tomita, K. Matsubara, Y. Okazaki, T. Ishii, Y. Oguma, I. Takei, and T. Saruta. 2002. Effects of pioglitazone on metabolic parameters, body fat distribution, and serum adiponectin levels in Japanese male patients with type 2 diabetes. *Metabolism* 51: 314–317.
53. Park, P. H., M. R. McMullen, H. Huang, V. Thakur, and L. E. Nagy. 2007. Short-term treatment of RAW264.7 macrophages with adiponectin increases tumor necrosis factor-α (TNF-α) expression via ERK1/2 activation and Egr-1 expression: role of TNF-α in adiponectin-stimulated interleukin-10 production. *J. Biol. Chem.* 282: 21695–21703.
54. Wijesekara, N., M. Krishnamurthy, A. Bhattacharjee, A. Suhail, G. Sweeney, and M. B. Wheeler. 2010. Adiponectin-induced ERK and Akt phosphorylation protects against pancreatic β cell apoptosis and increases insulin gene expression and secretion. *J. Biol. Chem.* 285: 33623–33631.
55. Turchi, L., A. A. Chassot, R. Rezzonico, K. Yeow, A. Loubat, B. Ferrua, G. Lenegrate, J. P. Ortonne, and G. Ponzio. 2002. Dynamic characterization of the molecular events during in vitro epidermal wound healing. *J. Invest. Dermatol.* 119: 56–63.
56. Yano, S., M. Komine, M. Fujimoto, H. Okochi, and K. Tamaki. 2004. Mechanical stretching in vitro regulates signal transduction pathways and cellular proliferation in human epidermal keratinocytes. *J. Invest. Dermatol.* 122: 783–790.
57. Xu, K. P., Y. Li, A. V. Ljubimov, and F. S. Yu. 2009. High glucose suppresses epidermal growth factor receptor/phosphatidylinositol 3-kinase/Akt signaling pathway and attenuates corneal epithelial wound healing. *Diabetes* 58: 1077–1085.
58. Zeigler, M. E., Y. Chi, T. Schmidt, and J. Varani. 1999. Role of ERK and JNK pathways in regulating cell motility and matrix metalloproteinase 9 production in growth factor-stimulated human epidermal keratinocytes. *J. Cell. Physiol.* 180: 271–284.

Diabetologia (2012) 55:3382–3391
DOI 10.1007/s00125-012-2703-1

ARTICLE

Protection from non-alcoholic steatohepatitis and liver tumourigenesis in high fat-fed insulin receptor substrate-1-knockout mice despite insulin resistance

A. Nakamura · K. Tajima · K. Zolzaya · K. Sato · R. Inoue · M. Yoneda · K. Fujita · Y. Nozaki · K. C. Kubota · H. Haga · N. Kubota · Y. Nagashima · A. Nakajima · S. Maeda · T. Kadowaki · Y. Terauchi

Received: 28 May 2012 / Accepted: 27 July 2012 / Published online: 7 September 2012

Abstract
Aims/hypothesis Epidemiological studies have revealed that obesity and diabetes mellitus are independent risk factors for the development of non-alcoholic steatohepatitis (NASH) and hepatocellular carcinoma. However, the debate continues on whether insulin resistance as such is directly associated with NASH and liver tumourigenesis. Here, we investigated the incidence of NASH and liver tumourigenesis in *Irs1*$^{-/-}$ mice subjected to a long-term high-fat (HF) diet. Our hypothesis was that hepatic steatosis, rather than insulin resistance may be related to the pathophysiology of these conditions.
Methods Mice (8 weeks old, C57Bl/6J) were given free access to standard chow (SC) or an HF diet. The development of NASH and liver tumourigenesis was evaluated after mice had been on the above-mentioned diets for 60 weeks. Similarly, *Irs1*$^{-/-}$ mice were also subjected to an HF diet for 60 weeks.
Results Long-term HF diet loading, which causes obesity and insulin resistance, was sufficient to induce NASH and liver tumourigenesis in the C57Bl/6J mice. Obesity and insulin resistance were reduced by switching mice from the HF diet to SC, which also protected these mice against the development of NASH and liver tumourigenesis. However, compared with wild-type mice fed the HF diet, *Irs1*$^{-/-}$ mice fed the HF diet were dramatically protected against NASH and liver tumourigenesis despite the presence of severe insulin resistance and marked postprandial hyperglycaemia.
Conclusions/interpretation IRS-1 inhibition might protect against HF diet-induced NASH and liver tumourigenesis, despite the presence of insulin resistance.

Keywords High-fat diet · Insulin receptor substrate-1 · Insulin resistance · Liver tumourigenesis · Non-alcoholic steatohepatitis

Abbreviations

ALT	Alanine aminotransferase
HCC	Hepatocellular carcinoma
H&E	Haematoxylin and eosin
HF	High-fat
HOMA-IR	HOMA of insulin resistance

A. Nakamura and K. Tajima contributed equally to this work.

Electronic supplementary material The online version of this article (doi:10.1007/s00125-012-2703-1) contains peer-reviewed but unedited supplementary material, which is available to authorised users.

A. Nakamura · K. Tajima · K. Zolzaya · K. Sato · R. Inoue · Y. Terauchi (✉)
Department of Endocrinology and Metabolism,
Graduate School of Medicine, Yokohama City University,
3-9 Fukuura, Kanazawa-ku,
Yokohama 236-0004, Japan
e-mail: terauchi-tky@umin.ac.jp

M. Yoneda · K. Fujita · Y. Nozaki · A. Nakajima · S. Maeda
Division of Gastroenterology, Graduate School of Medicine,
Yokohama City University,
Yokohama, Japan

K. C. Kubota · H. Haga
Department of Surgical Pathology, Hokkaido University Hospital,
Sapporo, Japan

N. Kubota · T. Kadowaki
Department of Diabetes and Metabolic Diseases,
Graduate School of Medicine, University of Tokyo,
Tokyo, Japan

Y. Nagashima
Department of Molecular Pathology,
Graduate School of Medicine, Yokohama City University,
Yokohama, Japan

NAFLD	Non-alcoholic fatty liver disease
NASH	Non-alcoholic steatohepatitis
PI3K	Phosphoinositide 3-kinase
SC	Standard chow

Introduction

The prevalence of obesity and diabetes has been increasing globally over the past 30 years [1, 2]. These diseases not only increase cardiovascular risk, but also cancer risk and mortality rates [3, 4]. Especially, hepatocellular carcinoma (HCC), the fifth most common cancer and the third leading cause of cancer death worldwide [5], accounts for the largest increase in cancer and mortality risk in individuals with obesity or diabetes [3, 4]. Certain cases of HCC may be associated with infection with hepatitis B or C virus, or chronic alcohol use. However, an increasing number of cases are associated with non-alcoholic fatty liver disease (NAFLD). NAFLD encompasses a clinicopathological spectrum of diseases ranging from isolated hepatic steatosis to non-alcoholic steatohepatitis (NASH), the more aggressive form of fatty liver disease, which may progress to cirrhosis and cirrhosis-related complications including HCC. The prevalence of NAFLD, including NASH, is also increasing in parallel with the growing obesity and diabetes epidemics [5].

Although the causal relationships between obesity or diabetes, and NASH or liver tumourigenesis have not yet been clearly elucidated, it is assumed that the insulin resistance associated with obesity and diabetes is involved in the development of hepatic steatosis and inflammation in the liver, which may progress to NASH and liver tumourigenesis [5]. Indeed, long-term high-fat (HF) diet loading, which can induce obesity and insulin resistance, was sufficient to induce NASH and liver tumourigenesis in C57Bl/6J mice [6–8]. Thus, this experimental model supports the above-mentioned concept.

IRS-1 and -2 exhibit a high structural homology, are abundantly produced in the liver and are thought to be responsible for transmitting insulin signalling from the insulin receptor to intracellular effectors in the regulation of glucose and lipid homeostasis [9, 10]. Insulin receptor signalling can be almost exclusively mediated by IRS-1 and IRS-2 in the liver [10]; indeed, a dominant role of IRS-1 has been observed during nutrient excess [11]. Moreover, HF diet-fed liver-specific *Irs1*$^{-/-}$ mice displayed severe insulin resistance, but not hepatic steatosis [11]. Also, mice with acyl-CoA:diacylglycerol acyltransferase (DGAT)2 overabundance in the liver reportedly developed hepatic steatosis without abnormal plasma glucose and insulin levels [12], while liver-specific phosphoinositide 3-kinase (PI3K) p110α-knockout (*Pik3ca*$^{-/-}$) mice fed an HF diet were protected against hepatic steatosis without ameliorating HF diet-induced glucose intolerance [13]. Mice with genetic defects or targeted overexpression, such as hepatocyte-specific *Pten*-knockout mice and *Pik3ca* transgenic mice [14, 15], have been reported to be models of NAFLD and liver tumourigenesis, but might not reflect the natural aetiology of NASH and liver tumourigenesis in human participants. Rather, insulin sensitivity was improved in hepatocyte-specific *Pten*-knockout mice, compared with wild-type mice [14], and *Pik3ca* transgenic mice exhibited better glucose tolerance than wild-type mice [15]. Therefore, liver steatosis can occur independently of insulin resistance.

In the present study, we investigated the effect of a long-term HF diet on the development of NASH and liver tumourigenesis using C57Bl/6J male mice. Next, we performed similar experiments in which the HF diet was switched to a standard chow (SC) diet to clarify the effect of improved insulin resistance on the development of these diseases. We also investigated the incidence of NASH and liver tumourigenesis in *Irs1*$^{-/-}$ mice subjected to a long-term HF diet. The hypothesis behind this part of the study was that hepatic steatosis, rather than insulin resistance, may be related to the pathophysiology of these conditions.

Methods

Animals Mice (*Irs1*$^{-/-}$) were generated as described elsewhere [16]. We backcrossed these mice with C57Bl/6J mice more than nine times. Male littermates derived from the intercrosses were fed an SC diet until 8 weeks of age and then had free access to the SC diet or an HF diet. In the dietary switch experiment, 8-week-old C57Bl/6J male mice were subjected to the HF diet for 30 weeks and then switched to the SC diet for the next 30 weeks; these mice were then compared with mice from the same genetic background that had received the HF diet for the entire 60 weeks. The mice were housed under a 12 h light–dark cycle. The animals were maintained according to standard animal care procedures based on institutional guidelines. These experiments involving animals were approved by the local Ethics Committee of the Yokohama City University.

Diet protocol We used an SC diet (MF; Oriental Yeast, Tokyo, Japan) and an HF diet (High-Fat Diet 32; Clea Japan, Tokyo, Japan). The composition of each of these diets is shown in electronic supplementary material (ESM) Table 1. The fatty acid composition of the HF diet consisted of 22% (wt/wt) saturated fatty acid (12.6% palmitic acid, 7.5% stearic acid) and 77% (wt/wt) unsaturated fatty acid (64.3% oleic acid, 10.2% linoleic acid).

Measurement of biochemical variables Blood glucose levels were measured using a portable glucose meter and Glutest Neo (Sanwa Chemical, Nagoya, Japan). Insulin levels were determined using an insulin ELISA kit (Morinaga, Yokohama,

Japan). Plasma alanine aminotransferase (ALT) levels were assayed using an enzymatic method (Wako Pure Chemical, Osaka, Japan). The plasma levels of total adiponectin and leptin were measured using ELISAs (Otsuka Pharmaceutical, Tokyo, Japan, and Morinaga, respectively). The triacylglycerol content of the liver was determined as described elsewhere [10]. HOMA of insulin resistance (HOMA-IR) was calculated by using the formula [fasting insulin (mU/l)×fasting plasma glucose (mmol/l)] / 22.5. When insulin is expressed in SI units as pmol/l, the constant changes to 156.26.

Glucose tolerance test Mice were denied access to food for more than 16 h before the study and then orally loaded with glucose at 1.5 mg/g body weight. Blood samples were collected before, and at 15, 30, 60 and 120 min after glucose loading.

Insulin tolerance test The insulin tolerance test was performed under non-fasting conditions. Insulin was injected intraperitoneally, and blood samples were collected before, and at 30, 60, 90 and 120 min after the injection.

Histopathological evaluation Liver samples were immersion-fixed overnight in 10% formalin (vol./vol.) at 4°C. The tissues were then routinely processed for paraffin embedding, and 5 μm sections mounted on glass slides were processed for haematoxylin and eosin (H&E) staining. The presence of collagen, which can be used as an index of fibrosis in lesions, was examined using Masson trichrome-stained preparations.

Liver histology and scoring system All the histopathological findings were scored by experienced pathologists, who were unaware of the genetic backgrounds and diets of the mice. The histological features were grouped into three broad categories: steatosis, inflammation and fibrosis. The scoring system used for the evaluation is detailed in ESM Table 2.

RNA preparation and real-time quantitative PCR Total RNA was prepared from portions of the liver using a reagent (Isogen; NipponGene, Tokyo, Japan), according to the manufacturer's instructions, and these samples were used as the starting material for cDNA preparations. cDNA was synthesised using reagents (TaqMan Reverse Transcription; Applied Biosystems, Foster City, CA, USA), followed by TaqMan quantitative PCR (50°C for 2 min and 95°C for 10 min, followed by 40 cycles at 95°C for 15 s and at 60°C for 1 min), performed on a PCR instrument (ABI Prism 7500; Applied Biosystems) to amplify the following genes: *Pparg*, *Srebp1c* (also known as *Srebf1*), *Fas*, *Scd1*, *Ppara*, *Cpt1* (also known as *Cpt1a*), *Mcad* (also known as *Acadm*), *Tnfa* (also known as *Tnf*), *Mcp1* (also known as *Ccl2*), *p22phox* (also known as *Cyba*), *gp91phox* (also known as *Cybb*), *p47phox* (also known as *Ncf1*) and *Irs2*. The relative expression levels were then compared after normalisation to the expression of beta-actin.

Statistical analysis Results are expressed as means ± SEM (*n*). Differences between two groups were analysed for statistical significance using Student's *t* test. Individual comparisons among four groups were performed using an ANOVA followed by Fisher's protected least significant difference post-hoc test. Also, individual comparisons between two time points and two groups were performed using a two-way ANOVA. A value of $p<0.05$ was considered statistically significant.

Results

Effects of long-term HF diet on metabolic changes in C57Bl/6J mice First, we tested the effect of long-term HF diet loading on the development of NASH and liver tumourigenesis in C57Bl/6J male (wild-type) mice. After 30 and 60 weeks on the HF diet, this mouse model showed higher body weights, fasting blood glucose levels, liver weights and plasma ALT levels than mice fed SC, but the plasma ALT levels were not significantly higher, presumably because of an interaction effect (Fig. 1a–d). The triacylglycerol content of the liver tended to be higher in wild-type mice after 30, but not after 60 weeks on the HF diet, compared with that in mice fed the SC diet (Fig. 1e). The glucose-lowering effect of insulin was impaired in this mouse model when fed the HF diet, compared with that in the same mouse model on the SC diet (Fig. 1f). Thus, the long-term administration of an HF diet induced obesity and insulin resistance in C57Bl/6J male mice. Furthermore, fasting insulin levels, HOMA of insulin resistance (HOMA-IR) and leptin levels were significantly higher, while plasma adiponectin levels were significantly lower in animals fed the HF diet than in those fed the SC diet (Fig. 1g–j), consistent with the results of previous reports [17, 18].

Effects of long-term HF diet on the risk of occurrence of NASH and liver tumourigenesis in C57Bl/6J mice Livers from wild-type mice fed the HF diet for 60 weeks were enlarged, compared with those in animals fed the SC diet for the same duration (Fig. 2a). Whereas wild-type mice on the SC diet had an almost normal liver histology (Fig. 2b, e), those fed the HF diet had typical features of NASH (Fig. 2c) at various stages of progression in the liver, including portal inflammation (Fig. 2d) and blue wave-like bands of fibrotic tissue in portal lesions (Fig. 2f, g). Scoring of the pathological findings showed significant increases for liver steatosis, inflammation and fibrosis in wild-type mice fed the HF diet, compared with scores in their counterparts on the SC diet (Fig. 2h). The expression of lipogenic genes, such as *Fas* and *Scd1*, after 30 weeks (Fig. 2i), and of genes encoding

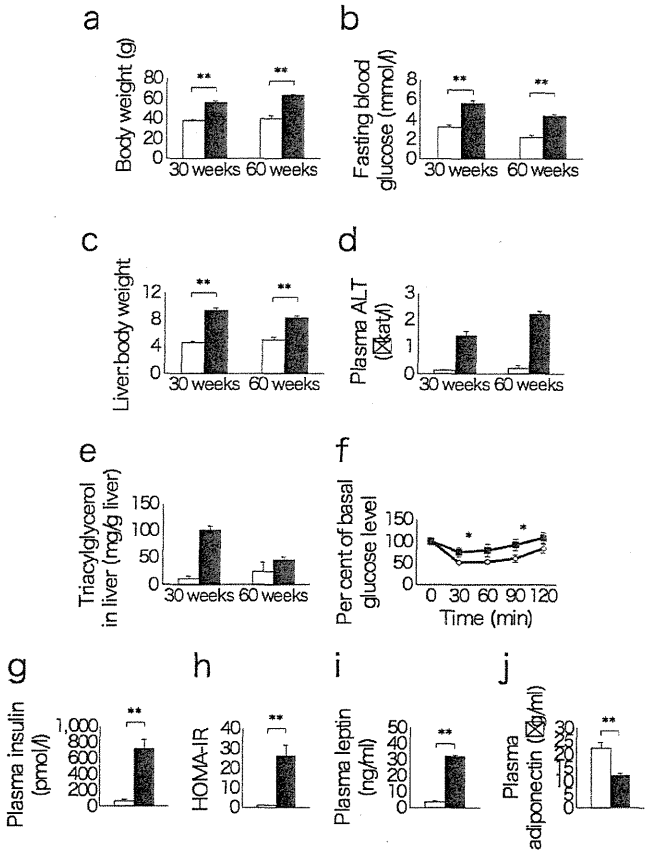

Fig. 1 Effects of a long-term HF diet on metabolic changes in C57Bl/6J mice. (**a**) Body weight, (**b**) fasting blood glucose, (**c**) ratio of liver: body weight, (**d**) plasma ALT and (**e**) triacylglycerol content of liver in mice fed the SC (white bars) or HF (black bars) diet for 30 or 60 weeks (n 8–24). (**f**) Insulin tolerance test in mice fed the SC (white diamonds) or HF (black squares) diet for 60 weeks (n 6). (**g**) Plasma fasting insulin levels, (**h**) HOMA-IR calculated from fasting blood glucose and insulin levels, (**i**) leptin levels and (**j**) total adiponectin levels in mice fed the SC or HF diet for 30 weeks (n 10–11). Values are mean ± SEM; *p<0.05 and **p<0.01

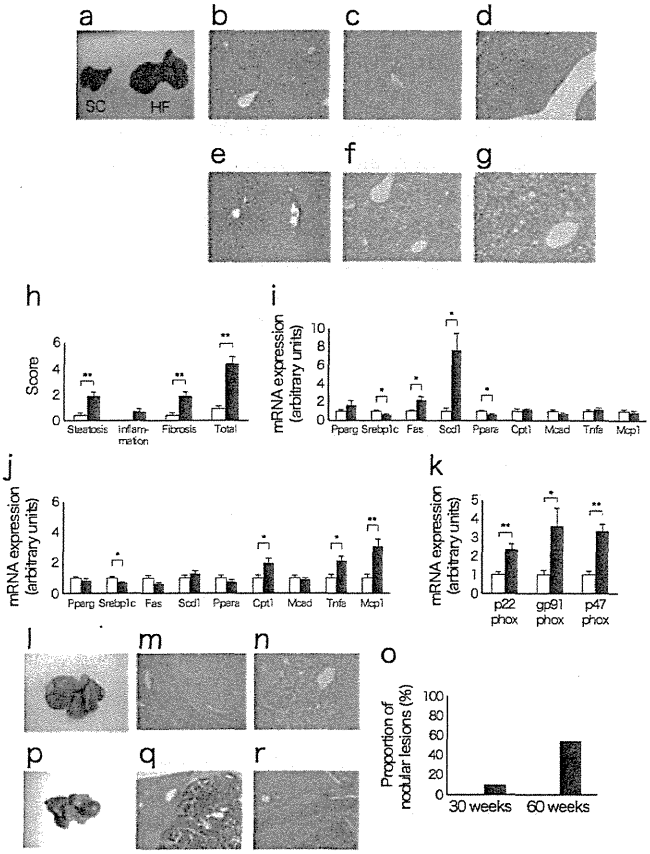

Fig. 2 Effects of a long-term HF diet on the risk of NASH and liver tumourigenesis in C57Bl/6J mice. (**a**) Macroscopic findings after 60 weeks. (**b, e**) Histopathological findings in the livers of mice fed the SC or HF (**c, d, f, g**) diets, as assessed using H&E- (**b**–**d**) and Masson trichrome (**e**–**g**)-stained sections. (**h**) The NASH/NAFLD Clinical Research Network scoring system definition and scores [32] for mice fed the SC (white bars) or HF (black bars) diet (n 9). (**i**) mRNA expression of lipogenic and inflammatory cytokine-related genes as listed after 30 and 60 (**j**) weeks, and (**k**) of genes encoding the reduced-form NADPH oxidase complex after 60 weeks in mice fed the SC or HF diet (n 5–6). (**l**) Macroscopic and (**m, n**) histopathological findings in sections containing liver tumours, as assessed using H&E-stained sections from mice fed the HF diet for 60 weeks. (**o**) Proportion of hepatic nodular lesions in mice fed the SC or HF diet (n 8–24). (**p**) Macroscopic and (**q, r**) histopathological features as assessed using H&E-stained sections of hepatic tumours from mice fed the HF diet for 80 weeks. Values are mean ± SEM; *p<0.05 and **p<0.01

inflammatory cytokines, such as *Tnfa* and *Mcp1*, after 60 weeks (Fig. 2j) was significantly increased in wild-type mice fed the HF diet, compared with that in animals fed the SC diet. Furthermore, the expression of genes encoding the reduced-form NADPH oxidase complex was coordinately elevated after 60 weeks in mice fed the HF diet, compared with findings in animals fed the SC diet (Fig. 2k). These results reflect the natural course of NASH: in other words, healthy liver becomes steatotic, followed by an inflammatory process caused by cytokines and oxidative stress, which results in hepatocellular degeneration and fibrosis. Moreover, tumours of various diameters were frequently observed on the liver surface in the HF group (Fig. 2l). Pathologically, these tumours were dysplastic nodules, adenomas or well-differentiated carcinomas (Fig. 2m, n), consistent with the findings of previous reports [6, 7]. These nodular lesions were observed on the liver surface in 10% of animals after 30 weeks and in 54% of animals after 60 weeks of administration of the HF diet in wild-type mice. In contrast, no such nodular lesions were detected in mice fed the SC diet (Fig. 2o). Interestingly, HCCs, which are characterised by disrupted normal liver architecture and intravascular tumour embolism, were found in certain mice after 80 weeks on the HF diet (Fig. 2p–r). As a point of reference, no increase in the phosphorylation levels of c-Jun N-terminal kinase (JNK), extracellular signal-regulated kinase (ERK) or p38 were noted in wild-type mice fed the HF diet, compared with the levels in mice fed the SC diet (data not shown). These results indicate that the long-term HF diet loading was sufficient to induce NASH and liver tumourigenesis in wild-type mice.

Switching from the HF to the SC diet: effects on metabolic changes in C57Bl/6J mice Next, to evaluate the effects of nutrients on fat distribution within the body, the degree of insulin resistance, and the risk of NASH and liver tumourigenesis, we compared C57Bl/6J male mice that were fed the HF diet for 30 weeks, followed by 30 weeks on the SC diet, with mice from the same genetic background that were fed the HF diet for the entire 60 weeks. The mice that were switched from the HF diet to the SC diet showed a significantly lower body weight and visceral fat weight than the animals that were fed the HF diet for the entire 60 weeks, although no differences in fed-state blood glucose levels were observed between the two groups (Fig. 3a–d). The diet switch improved the degree of hyperinsulinaemia and insulin resistance, as evidenced by fasting insulin levels, HOMA-IR and insulin tolerance test results (Fig. 3e, f, ESM Fig. 1). The diet switch was also associated with a decrease in liver weight, plasma ALT levels and liver triacylglycerol content, although the difference for the latter was not statistically significant (Fig. 3g–j).

Switching from the HF to the SC diet: effects on the incidence of NASH and liver tumourigenesis in C57Bl/6J mice Compared with the findings for mice that continued the HF diet for the entire 60 weeks, findings for mice that were switched from the HF to the SC diet showed an almost normal liver histology (Fig. 4a, b), with significantly decreased pathological scores for NASH (Fig. 4c). Also, the expression of genes encoding inflammatory cytokines such as *Tnfa* and *Mcp1*, and the reduced-form NADPH oxidase complex decreased significantly in the group that switched diets (Fig. 4d, e). The proportion of nodular lesions was also significantly decreased by the dietary switch (Fig. 4f). These findings suggest that the correction of nutrient conditions improved obesity and the related insulin resistance, and protected the animals against HF diet-induced NASH and liver tumourigenesis.

Effects of long-term HF diet on metabolic changes in Irs1$^{-/-}$ mice To evaluate the effect of hepatic steatosis on HF diet-induced NASH and liver tumourigenesis, we used *Irs1*$^{-/-}$ male mice, which exhibit postnatal growth retardation and insulin resistance, but have normal glucose tolerance because of compensatory beta cell hyperplasia [19–21]. As expected, the body weight of *Irs1*$^{-/-}$ mice was about two thirds that of wild-type mice in the SC and HF diet groups (Fig. 5a). However, fed-state blood glucose levels were increased in *Irs1*$^{-/-}$ mice, compared with those in wild-type mice, after 6 weeks on the HF diet, although no differences in fed-state glucose levels were observed between wild-type and *Irs1*$^{-/-}$ mice fed the SC diet (Fig. 5b). Interestingly, the liver weight, plasma ALT levels and triacylglycerol content of the liver were significantly higher in wild-type mice fed the HF diet than in the other groups of mice (Fig. 5c–e). Moreover, although wild-type

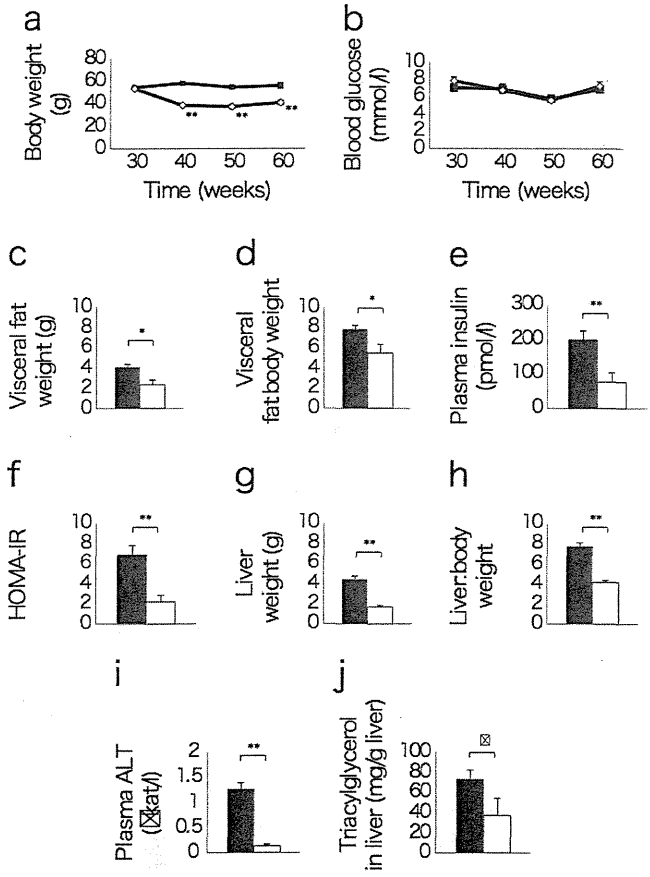

Fig. 3 Effects of the switch from the HF to the SC diet on metabolic changes in C57Bl/6J mice. The mice were fed the HF diet for 30 weeks, followed by the SC diet for 30 weeks. They were then compared with mice fed the HF diet for 60 weeks. (**a**) Changes in body weight and (**b**) fed-state blood glucose levels in the HF diet alone (black squares) and HF + SC diet (white diamonds) groups (n 10). (**c**) Visceral fat weight and (**d**) the ratio of visceral fat weight to body weight in the HF diet alone (black bars) and the HF + SC diet (white bars) groups (n 5). (**e**) Plasma fasting insulin, (**f**) HOMA-IR, (**g**) liver weight, (**h**) ratio of liver to body weight, (**i**) plasma ALT and (**j**) triacylglycerol content of the liver in the two groups of mice (n 10). Values are mean ± SEM; *p< 0.05 and **p<0.01; †p 0.08

mice fed the HF diet demonstrated the typical features of hepatic steatosis, the other three groups showed an almost normal liver histology (Fig. 5f–i). These results indicate that the disruption of IRS-1 protected against HF diet-induced hepatic steatosis.

Based on these results, we next compared the effects of long-term HF diet loading on metabolic changes in *Irs1*$^{-/-}$ mice relative to those in wild-type mice. Although the body weight of *Irs1*$^{-/-}$ mice was about two thirds that of wild-type mice and the visceral fat weight in the former was also lower (*Irs1*$^{-/-}$ mice 2.3±0.1 g vs wild-type 3.9±0.1 g), no difference in the ratio of visceral weight to body weight was observed between the two groups (Fig. 6a–c). The insulin and oral glucose tolerance tests revealed that *Irs1*$^{-/-}$ mice

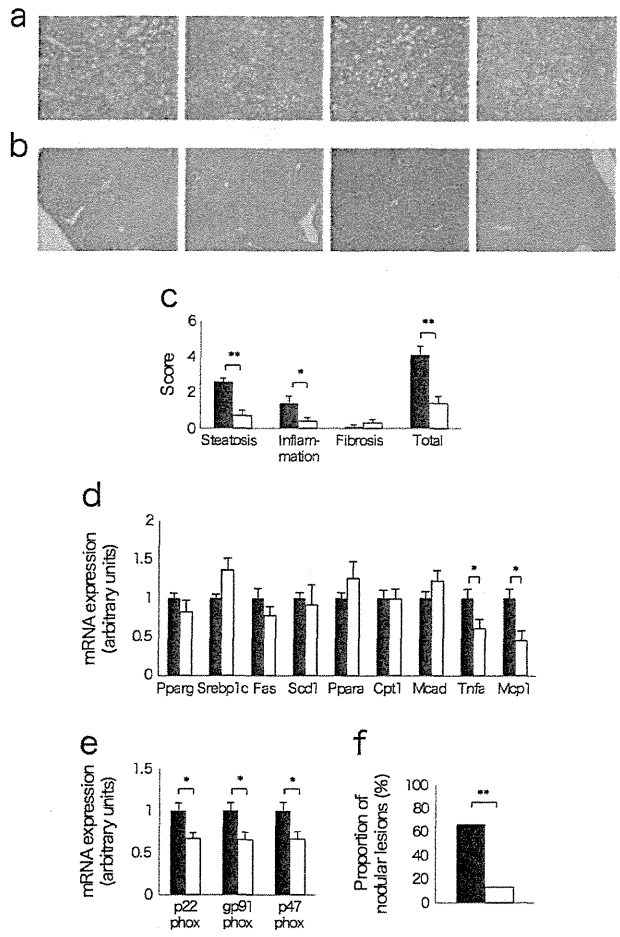

Fig. 4 Effects of switching from the HF to the SC diet on the incidence of NASH and liver tumourigenesis in C57Bl/6J mice. The mice were fed the HF diet for 30 weeks, followed by the SC diet for 30 weeks. They were then compared with mice fed the HF diet for 60 weeks. (**a**) Histopathological findings of NASH in the livers from the HF diet alone group and (**b**) the HF + SC diet group, as observed using H&E-stained sections (n 4). (**c**) NASH/NAFLD Clinical Research Network scoring system definitions and scores [32] for the HF diet alone (black bars) and the HF + SC diet (white bars) groups of mice (n 9–10). (**d**) mRNA expression of lipogenic and inflammatory cytokine-related genes, and (**e**) of genes encoding the reduced-form NADPH oxidase complex in the two groups of mice (n 4–6). (**f**) Proportion of hepatic nodular lesions in the two groups of mice (n 15). Values are mean ± SEM; *p<0.05 and **p<0.01

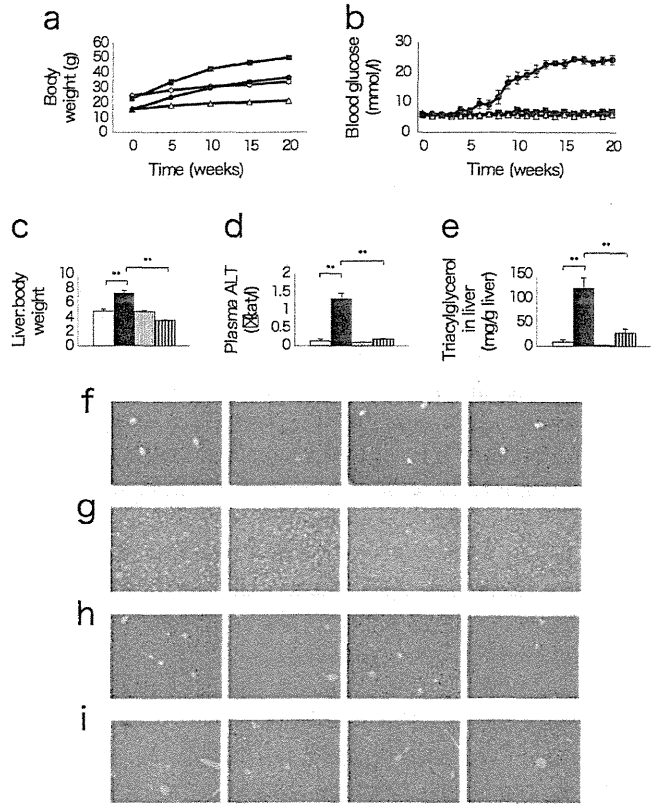

Fig. 5 Effects of an HF diet on liver steatosis in *Irs1*$^{-/-}$ mice. (**a**) Changes in the body weight and (**b**) fed-state blood glucose levels in wild-type and *Irs1*$^{-/-}$ mice fed the SC or HF diet (white diamonds, wild-type SC; black squares, wild-type HF; white triangles, *Irs1*$^{-/-}$ SC; black circles, *Irs1*$^{-/-}$ HF) (n 7–11). (**c**) Ratio of liver weight to body weight, (**d**) plasma ALT and (**e**) triacylglycerol content of the liver in mice as above (**a**, **b**) at 20 weeks of respective diet (white bars, wild-type SC; black bars, wild-type HF; dotted bars, *Irs1*$^{-/-}$ SC; striped bars, *Irs1*$^{-/-}$ HF) (n 5–10). (**f**) Histopathological findings in the livers of wild-type SC-, (**g**) wild-type HF-, (**h**) *Irs1*$^{-/-}$ SC- and (**i**) *Irs1*$^{-/-}$ HF-fed mice, as assessed using H&E-stained sections (n 4). Values are mean ± SEM; **p<0.01

fed the HF diet had severe insulin resistance and marked postprandial hyperglycaemia compared with wild-type mice on the same diet (Fig. 6d, e). Also, their fasting insulin levels and HOMA-IR values were significantly higher than in wild-type mice (Fig. 6f, g). Moreover, the liver weight, plasma ALT levels and triacylglycerol content of the liver were significantly lower in *Irs1*$^{-/-}$ mice than in wild-type mice fed the HF diet (Fig. 6a, h–j). Although no difference in plasma leptin levels was seen, adiponectin levels were significantly higher in *Irs1*$^{-/-}$ mice (Fig. 6k, l).

Effects of long-term HF diet on the incidence of NASH and liver tumourigenesis in Irs1$^{-/-}$ *mice* Apparently, *Irs1*$^{-/-}$ mice fed the HF diet showed an almost normal liver histology (Fig. 7a–d), while pathological scores for NASH were significantly lower in *Irs1*$^{-/-}$ mice (Fig. 7e). Also, the expression of lipogenic genes such as *Fas* and *Scd1* at 30 weeks, and of genes encoding inflammatory cytokines and the reduced-form NADPH oxidase complex at 60 weeks were significantly decreased in *Irs1*$^{-/-}$ mice on the HF diet, compared with wild-type mice fed the same diet (Fig. 7f–h). Moreover, the proportion of nodular lesions was significantly lower in *Irs1*$^{-/-}$ mice fed the HF diet than in wild-type mice on the same diet (Fig. 7i). These results indicate that the disruption of IRS-1 protected against HF diet-induced NASH and liver tumourigenesis, despite being associated with severe hyperglycaemia and insulin resistance.

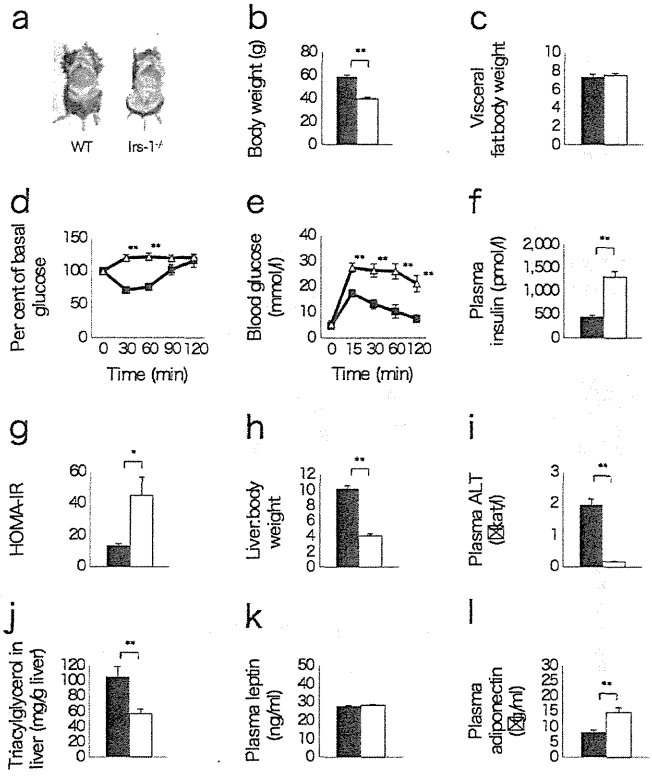

Fig. 6 Effects of a long-term HF diet on metabolic changes in *Irs1*$^{-/-}$ mice. (**a**) Macroscopic observation in wild-type (WT) and *Irs1*$^{-/-}$ mice fed the HF diet. (**b**) Body weight and (**c**) ratio of visceral weight to body weight in wild-type (black bars) and *Irs1*$^{-/-}$ (white bars) mice fed the HF diet for 30 weeks (n 4–10). (**d**) Insulin and (**e**) oral glucose tolerance tests in wild-type (black squares) and *Irs1*$^{-/-}$ (white triangles) mice fed the HF diet for 30 weeks (n 8–10). (**f**) Plasma fasting insulin, (**g**) HOMA-IR, (**h**) ratio of liver weight to body weight, (**i**) plasma ALT, (**j**) hepatic triacylglycerol content, (**k**) plasma leptin levels and (**l**) plasma total adiponectin levels in wild-type and *Irs1*$^{-/-}$ mice fed the HF diet for 30 weeks (n 6–10). Values are mean ± SEM; *p<0.05 and **p<0.01

Discussion

In the present study, we showed that long-term HF diet loading, which causes obesity and peripheral insulin resistance, was sufficient to induce NASH and liver tumourigenesis in C57Bl/6J mice, and that the reduction of obesity and peripheral insulin resistance by switching from the HF to an SC diet protected animals against the development of NASH and liver tumourigenesis. More importantly, the results of our study indicate that *Irs1*$^{-/-}$ mice fed the HF diet were dramatically protected against NASH and liver tumourigenesis, despite having severe insulin resistance and marked postprandial hyperglycaemia. These results are not consistent with the prevalent notion that the insulin resistance associated with obesity and diabetes is involved in the development of hepatic steatosis and inflammation in the liver, which may progress to NASH and liver tumourigenesis [5].

How can these results be explained? One explanation is the concept of selective or partial insulin resistance [22]. Thus humans with insulin resistance caused by inherited mutations in the insulin receptor and mice with a liver-specific deletion of the insulin receptor have hyperglycaemia and hyperinsulinaemia, but are both protected against hepatic steatosis and hypertriacylglycerolaemia [23, 24]. This finding is consistent with the idea that not all signals are blunted in classical insulin-resistant states; instead, some signals are preserved, particularly those related to hepatic steatosis.

Insulin receptor signalling can be almost exclusively mediated by IRS-1 and IRS-2 in the liver, with IRS-2 mainly functioning during fasting and immediately after re-feeding, while IRS-1 functions primarily after re-feeding [10]. In our results in wild-type mice, *Irs2* levels were significantly decreased in the HF diet group, compared with those in the SC diet group, under fasting conditions, while levels of *Irs1* in the HF diet group were similar to those in the SC diet group under re-feeding conditions (ESM Fig. 2). Insulin signalling might be decreased mainly under fasting conditions in the HF diet group, as the hyperinsulinaemia associated with an HF diet may suppress IRS-2 production [25]. In this case, HF diet feeding might place the mice in a chronic postprandial state that preferentially inactivates IRS-2, with persistent IRS-1 signalling possibly promoting lipogenesis and leading to hepatic steatosis, since IRS-1 has been proposed to be the dominant regulator of expression of the hepatic genes controlling lipogenesis [11]. In contrast, hepatic insulin signalling in *Irs1*$^{-/-}$ mice fed the HF diet was impaired, since IRS-1 was absent and IRS-2 signalling was suppressed by the hyperinsulinaemia associated with the HF diet. Thus, the pathophysiological features in *Irs1*$^{-/-}$ mice fed the HF diet might be similar to those in liver-specific *Irs1*/*Irs2* double-knockout mice and in liver-specific insulin receptor knockout mice [11, 24]. A similar situation is seen with the liver-specific loss-of-function of the p110α subunit of PI3K [13] or of Akt [26]. Since the IRS proteins lie between these steps [27], these previous studies using mouse models with genetic engineering of genes encoding the insulin receptor, IRS, PI3K and Akt are consistent with the phenotype of the *Irs1*$^{-/-}$ mice fed the HF diet in our study.

Importantly, the mice in the present study, unlike liver-specific knockout mice, had impaired IRS-1 functions in all their tissues. It thus remains unclear whether the protection against NASH and liver tumourigenesis is due to a global loss of insulin signalling or a liver-specific loss. Unfortunately, the current data do not answer this question. However, we assumed that the protection might be due to a liver-autonomous effect, since liver-specific *Irs1*$^{-/-}$ mice fed an HF diet, but not liver-specific *Irs2*$^{-/-}$ mice fed an HF diet were reportedly protected from hepatic steatosis [11] and the steatotic host microenvironment probably sets the stage for tumour development, even during the initially reversible and treatable stages of fatty liver disease [7]. Therefore, this